FINAL REPORT

November, 1990

A Compact Programmable Laser Doppler Velocimeter for Marine Applications

Contract Number 90-C-0105

Prepared for:

Dr. Joseph H. Kravitz
Office of Naval Research
800 N. Quincy Street
Arlington, Virginia 22217

Prepared by:

Dr. Cecil F. Hess
MetroLaser
18006 Skypark Circle Suite 108
Irvine, CA 92714

FINAL REPORT ON0101

1. INTRODUCTION

The purpose of this SBIR program is to research and develop a new laser Doppler velocimeter for deployment in the ocean. The system must be programmable and autonomous, and must operate unattended over periods of about six months. The system will ultimately operate in highly dynamic shallow water environments and must be capable of providing magnitude and direction of the velocity distribution in two directions and associated flow turbulence as a function of time. The system will be utilized to measure sediment motion and a variety of ocean transport phenomena in highly dynamic situations.

The choice of hardware was suggested in the Phase I proposal and has been implemented during the Phase I work. It included a laser diode to illuminate the particles, three Bragg cells to obtain velocity directionality and to separate the horizontal and vertical velocity components, an avalanche photodiode (APD) to collect the scattered light, a programmable digital signal processor (DSP) and solid state memory to record and process the velocity data, and optics to produce the measurement volume and collect the scattered light. All of these components were carefully chosen with the goal of satisfying the NAVY's requirements with the smallest possible system.

As indicated later in this report, the total power consumption of the final system would be about 10 watts during data acquisition, and 0.2 watts during the waiting periods. Total time of data acquisition during the six month period is expected to be about 24 hours. This operational time assumes that a velocity reading is made every hour on the hour. This time could be reduced if instead of collecting data at constant time intervals, a sensor such as a microphone or an accelerometer was used to activate the velocimeter during times of vigorous activity. The data acquisition logic will be decided in close consultation with NAVY technical personnel.

During the performance of the Phase I work we compared the capabilities of a pulsed laser diode configuration with those of a continuous wave laser diode and concluded that no major advantages were obtained by pulsing the laser diode. This conclusion would have been different if a different family of lasers had been considered (such as YAG). However the power limitations imposed by a battery operated system clearly define the laser diode as the best candidate and we therefore chose it for our work.

The velocity of the water flow was measured in a test cell oriented both horizontally and tilted 34 degrees from the horizontal. The vertical and horizontal velocity components were simultaneously measured thus providing the magnitude of the velocity as well as the direction traveled by each particle crossing the probe volume. The light scattered by these particles was collected by lenses and directed to an avalanche photodiode where it was converted into an electronic signal. This electronic signal was amplified and stored in solid state memory for after-processing. FFTs were performed by the programmable digital signal processor providing the frequency spectrum which separated the two components of the velocity. The frequency resolution using a 100 MHz A/D converter was estimated at 2.5 KHz which corresponded to 0.07 m/s. For a velocity of 7 m/s this represents a resolution of 1%. The frequency of the A/D clock could be varied to optimize the resolution of a particular frequency range. This resolution could also be enhanced by algorithms which include skipping and multiple FFTs. Velocity resolution between 0.1% and 0.5% should thus be possible.

Recent discussions with the technical program monitor indicate that measuring the particle size would considerably enhance the capability of the system. It is our opinion and recommendation that such capability could be added to the probe without a substantial increase in its complexity. This stems from the fact that the processor is programmable and could incorporate additional algorithms.

2. BACKGROUND AND THEORY

The LDV transmitter produced three laser beams which crossed to form the probe volume. Particles traveling though this probe volume scattered light which contained the velocity information. This scattered light was collected by a receiver, transformed by an APD into an electronic signal with similar time and amplitude variations, and digitized and stored by the electronic processor. To measure two velocity components each of the three laser beams was frequency shifted by a Bragg cell such that the difference in frequency between any two beams was unique and separable in the frequency domain. Figure 1 shows the three laser beam configuration while Figure 2 shows a schematic of the breadboard used in Phase I. As indicated on Figure 1, the three frequencies were: 75, 80, and 90 MHz, which produced frequency differences of 5, 10, and 15 MHz. Thus the horizontal velocity component had a frequency shift (fs_1) of 5 MHz, the vertical velocity component had a frequency shift (fs_2) of 10 MHz, and the 15 MHz shift corresponded to a diagonal velocity component which was discarded. A stationary particle positioned in the probe volume would scatter light which contained all three frequencies. As the particles moved due to flow velocity, the processed frequencies would be:

$$f_1 = fs_1 \pm U/\delta_1, \tag{1}$$

$$f_2 = fs_2 \pm V/\delta_2, \tag{2}$$

where f_1 and f_2 are the processed frequencies, δ_1 and δ_2 are the fringe spacings, and U and V are the velocity components in the horizontal and vertical directions. The values of δ_1 and δ_2 were 28 μm and 25 μm respectively. U/δ is referred to as the Doppler frequency and its sign can be easily established by comparing f to fs.

The above theory leads to the conclusion that a single photodetector and a single electronic processor can provide the velocity magnitude and direction in two axes. This was successfully demonstrated with the Phase I system. The constraint imposed by this system is that f_1 and f_2 must be separable in the frequency spectrum. This can be easily met in ocean applications since the velocities are very slow. A very conservative design would require that the difference between f_1 and f_2 be four times the maximum expected Doppler frequency.

The Phase I design was based on a maximum velocity of 10 m/s crossing a 25 μm fringe spacing, therefore yielding a Doppler frequency of 0.4 MHz. Thus, the difference between processed frequencies, must be $f_1 - f_2 = 1.6$ MHz. This can be achieved with Bragg cells operating at 80 MHz, 81.6 MHz, and 84.8 MHz. The maximum processed frequency would then be 5.2 MHz (for a 0.4 MHz shift) and the minimum frequency would be 1.2 MHz. A 20 MHz digitizer would exceed the requirements imposed by Nyquist limit, and provide excellent velocity resolution. During Phase I we used a 100 MHz digitizer which is much faster than necessary and uses more power than a 20 MHz digitizer, which according to this simple analysis would be more adequate for the Phase II system.

For most ocean applications the velocity would be even slower than the value assumed above; probably in the order of cm/s. In this case the digitizer could be much slower than the chosen 20 MHz resulting in even lower power consumption.

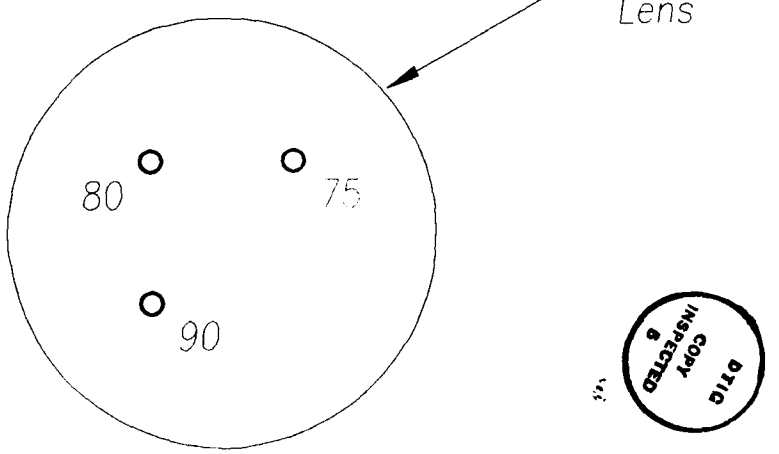

Statement "A" per telecon Dr. Joseph Kravitz. Office of Naval Research/ code 1125GG.

VHG 11/20/90

Figure 1. Three beam configuration.

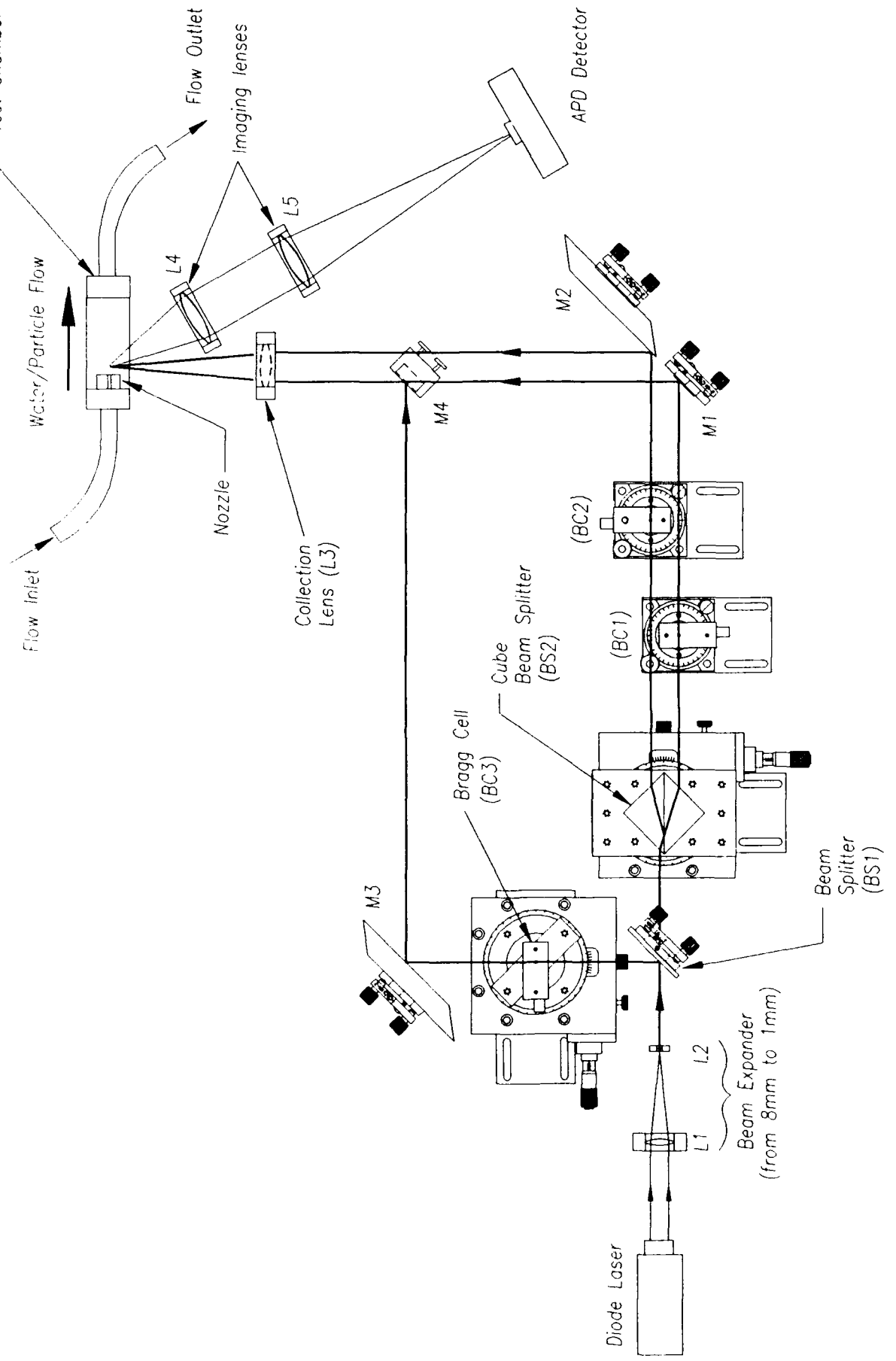

Figure 2. Phase I breadboard.

Mie scattering solutions

The scattering cross-section of particles between approximately 2 and 20 microns in diameter were computed for three indices of refraction and two collection angles. The indices of refraction were 1.05, 1.1, and 1.2 which according to the literature are fairly typical of particles found in the ocean. The angles of collection were 160 and 180 degrees. While the Phase II system would operate at 180 degrees, the Phase I collection angle was chosen as 160. This was due to the fact that we were short of one beam splitter to implement the 180 degree configuration. For the purposes of system evaluation it makes little difference since the scattering cross-section is of the same order magnitude for the two collection angles. The other parameters which influence the scattering cross-section are the laser wavelength, the F/# of the receiving lens, and the polarization of the incident beam. These parameters are listed with the results.

The results are given on Tables 1 through 6 and on Figures 3 and 4. These results were used in predicting signal to noise ratios. It is evident from these figures, that the scattered light intensity collected in back scattering is a strong function of index of refraction. This combined with the nonpherical shape of the particles precludes accurate particle sizing using backscatting. An on-axis configuration would collect light which is scattered by diffraction which is more insensitive to shape and index of refraction and would therefore yield more accurate results. Appendix A and B show possible schemes which would provide the particle velocity and size distributions. It is shown that for angles of collection near on-axis (zero degrees) the intensity of the scattered light is reasonably independent of index of refraction.

```
DATA FILENAME :on120160
LENS DIAMETER IN (MM) =   20.000
NUMBER OF INTEGRATION ALONG RADIUS & PI =      5      5
LENS CENTER DISTANCE IN (MM) =   50.000
LENS CENTER ANGLE IN (DEGREE) =  160.000
LASER WAVELENGTH IN (MICRON) =    .8150
LASER POLA TO X (X TO Y) IN (DEGREE)=   90.000
INDEX OF REFRACTION =    1.200     .000
----------------------------------------
F(1) : RESPONSE FUNCTION
I/I0 : RATIO OF SCATTER TO INCIDENT INTENSITY
       CROSS SECTION (1.0E-8 CM^2)
----------------------------------------
SIZE PARA.   DIAM.(MICRON)    F(1)            I/I0
 10.0000      2.5942         .1415E+00       .2380E-02
 20.0000      5.1885         .2661E+01       .4477E-01
 30.0000      7.7827         .5932E+01       .9981E-01
 40.0000     10.3769         .8399E+01       .1413E+00
 50.0000     12.9711         .2166E+02       .3644E+00
 60.0000     15.5654         .1147E+02       .1930E+00
 70.0000     18.1596         .3338E+02       .5617E+00
 80.0000     20.7538         .2816E+02       .4739E+00
```

Table 1. Mie scattering computations for particles with an index of refraction of 1.2 collected at 160 degrees.

```
DATA FILENAME :on110160
LENS DIAMETER IN (MM) =   20.000
NUMBER OF INTEGRATION ALONG RADIUS & PI =      5      5
LENS CENTER DISTANCE IN (MM) =   50.000
LENS CENTER ANGLE IN (DEGREE) =  160.000
LASER WAVELENGTH IN (MICRON) =    .8150
LASER POLA TO X (X TO Y) IN (DEGREE)=   90.000
INDEX OF REFRACTION =    1.100     .000
----------------------------------------
F(1) : RESPONSE FUNCTION
I/I0 : RATIO OF SCATTER TO INCIDENT INTENSITY
       CROSS SECTION (1.0E-8 CM^2)
----------------------------------------
SIZE PARA.   DIAM.(MICRON)    F(1)            I/I0
 10.0000      2.5942         .3949E-01       .6644E-03
 20.0000      5.1885         .9905E-01       .1666E-02
 30.0000      7.7827         .2639E+00       .4441E-02
 40.0000     10.3769         .9807E+00       .1650E-01
 50.0000     12.9711         .2854E+01       .4802E-01
 60.0000     15.5654         .6725E+01       .1131E+00
 70.0000     18.1596         .1181E+02       .1988E+00
 80.0000     20.7538         .2048E+02       .3447E+00
```

Table 2. Mie scattering computations for particles with an index of refraction of 1.1 collected at 160 degrees.

```
DATA FILENAME :on105160
LENS DIAMETER IN (MM) =    20.000
NUMBER OF INTEGRATION ALONG RADIUS & PI =       5       5
LENS CENTER DISTANCE IN (MM) =    50.000
LENS CENTER ANGLE IN (DEGREE) =  160.000
LASER WAVELENGTH IN (MICRON) =     .8150
LASER POLA TO X (X TO Y) IN (DEGREE)=    90.000
INDEX OF REFRACTION =     1.050      .000
----------------------------------------
F(1) : RESPONSE FUNCTION
I/I0 : RATIO OF SCATTER TO INCIDENT INTENSITY
       CROSS SECTION (1.0E-8 CM^2)
----------------------------------------
SIZE PARA.   DIAM.(MICRON)    F(1)             I/I0
 10.0000      2.5942         .9050E-03        .1523E-04
 20.0000      5.1885         .2273E-01        .3824E-03
 30.0000      7.7827         .3192E-01        .5371E-03
 40.0000     10.3769         .5256E-01        .8843E-03
 50.0000     12.9711         .1078E+00        .1814E-02
 60.0000     15.5654         .1442E+00        .2426E-02
 70.0000     18.1596         .1878E+00        .3160E-02
 80.0000     20.7538         .3363E+00        .5658E-02
```

Table 3. Mie scattering computations for particles with an index of refraction of 1.05 collected at 160 degrees.

```
DATA FILENAME :on120180
LENS DIAMETER IN (MM) =    20.000
NUMBER OF INTEGRATION ALONG RADIUS & PI =       5       5
LENS CENTER DISTANCE IN (MM) =    50.000
LENS CENTER ANGLE IN (DEGREE) =  180.000
LASER WAVELENGTH IN (MICRON) =     .8150
LASER POLA TO X (X TO Y) IN (DEGREE)=    90.000
INDEX OF REFRACTION =     1.200      .000
----------------------------------------
F(1) : RESPONSE FUNCTION
I/I0 : RATIO OF SCATTER TO INCIDENT INTENSITY
       CROSS SECTION (1.0E-8 CM^2)
----------------------------------------
SIZE PARA.   DIAM.(MICRON)    F(1)             I/I0
 10.0000      2.5942         .1146E+00        .1928E-02
 20.0000      5.1885         .7788E+01        .1310E+00
 30.0000      7.7827         .1741E+02        .2929E+00
 40.0000     10.3769         .3226E+02        .5427E+00
 50.0000     12.9711         .4843E+02        .8148E+00
 60.0000     15.5654         .3197E+02        .5380E+00
 70.0000     18.1596         .1245E+03        .2094E+01
 80.0000     20.7538         .1178E+03        .1982E+01
```

Table 4. Mie scattering computations for particles with an index of refraction of 1.2 collected at 180 degrees.

```
DATA FILENAME :on110180
LENS DIAMETER IN (MM) =   20.000
NUMBER OF INTEGRATION ALONG RADIUS & PI =      5      5
LENS CENTER DISTANCE IN (MM) =   50.000
LENS CENTER ANGLE IN (DEGREE) =  180.000
LASER WAVELENGTH IN (MICRON) =    .8150
LASER POLA TO X (X TO Y) IN (DEGREE)=   90.000
INDEX OF REFRACTION =    1.100     .000
----------------------------------------
F(1) : RESPONSE FUNCTION
I/I0 : RATIO OF SCATTER TO INCIDENT INTENSITY
       CROSS SECTION (1.0E-8 CM^2)
----------------------------------------
SIZE PARA.  DIAM.(MICRON)   F(1)            I/I0
 10.0000     2.5942         .5457E-01       .9182E-03
 20.0000     5.1885         .2808E+00       .4724E-02
 30.0000     7.7827         .9971E+00       .1678E-01
 40.0000    10.3769         .3010E+01       .5065E-01
 50.0000    12.9711         .7700E+01       .1296E+00
 60.0000    15.5654         .1744E+02       .2935E+00
 70.0000    18.1596         .3293E+02       .5541E+00
 80.0000    20.7538         .5105E+02       .8589E+00
```

Table 5. Mie scattering computations for particles with an index of refraction of 1.1 collected at 180 degrees.

```
DATA FILENAME :on105180
LENS DIAMETER IN (MM) =   20.000
NUMBER OF INTEGRATION ALONG RADIUS & PI =      5      5
LENS CENTER DISTANCE IN (MM) =   50.000
LENS CENTER ANGLE IN (DEGREE) =  180.000
LASER WAVELENGTH IN (MICRON) =    .8150
LASER POLA TO X (X TO Y) IN (DEGREE)=   90.000
INDEX OF REFRACTION =    1.050     .000
----------------------------------------
F(1) : RESPONSE FUNCTION
I/I0 : RATIO OF SCATTER TO INCIDENT INTENSITY
       CROSS SECTION (1.0E-8 CM^2)
----------------------------------------
SIZE PARA.  DIAM.(MICRON)   F(1)            I/I0
 10.0000     2.5942         .2668E-02       .4490E-04
 20.0000     5.1885         .7440E-02       .1252E-03
 30.0000     7.7827         .7256E-01       .1221E-02
 40.0000    10.3769         .3921E-01       .6597E-03
 50.0000    12.9711         .6340E-01       .1067E-02
 60.0000    15.5654         .3149E+00       .5298E-02
 70.0000    18.1596         .2171E+00       .3652E-02
 80.0000    20.7538         .3084E+00       .5189E-02
```

Table 6. Mie scattering computations for particles with an index of refraction of 1.05 collected at 180 degrees.

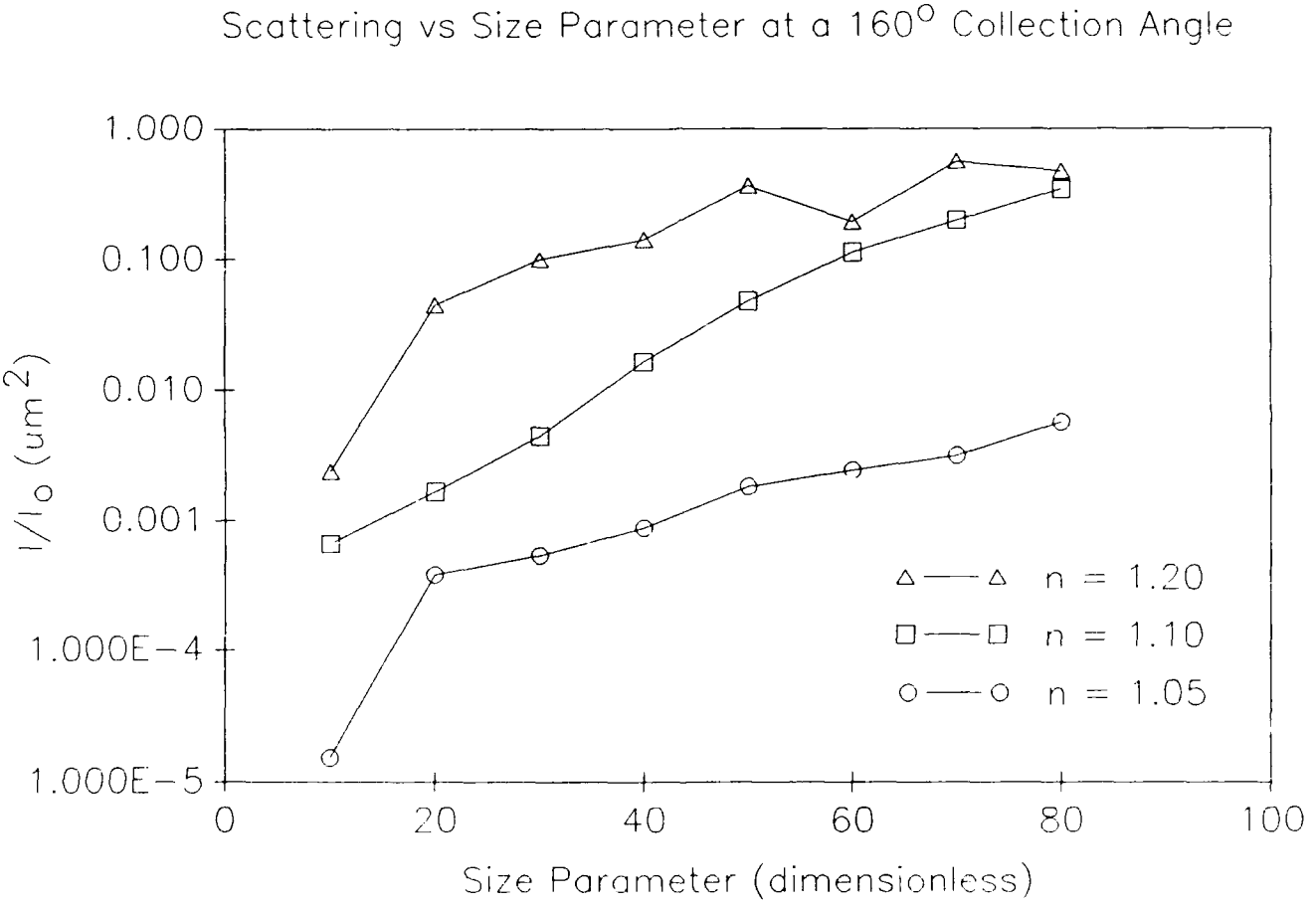

Figure 3. Mie scattering computations for particles with three indices of refraction collected at 160 degrees.

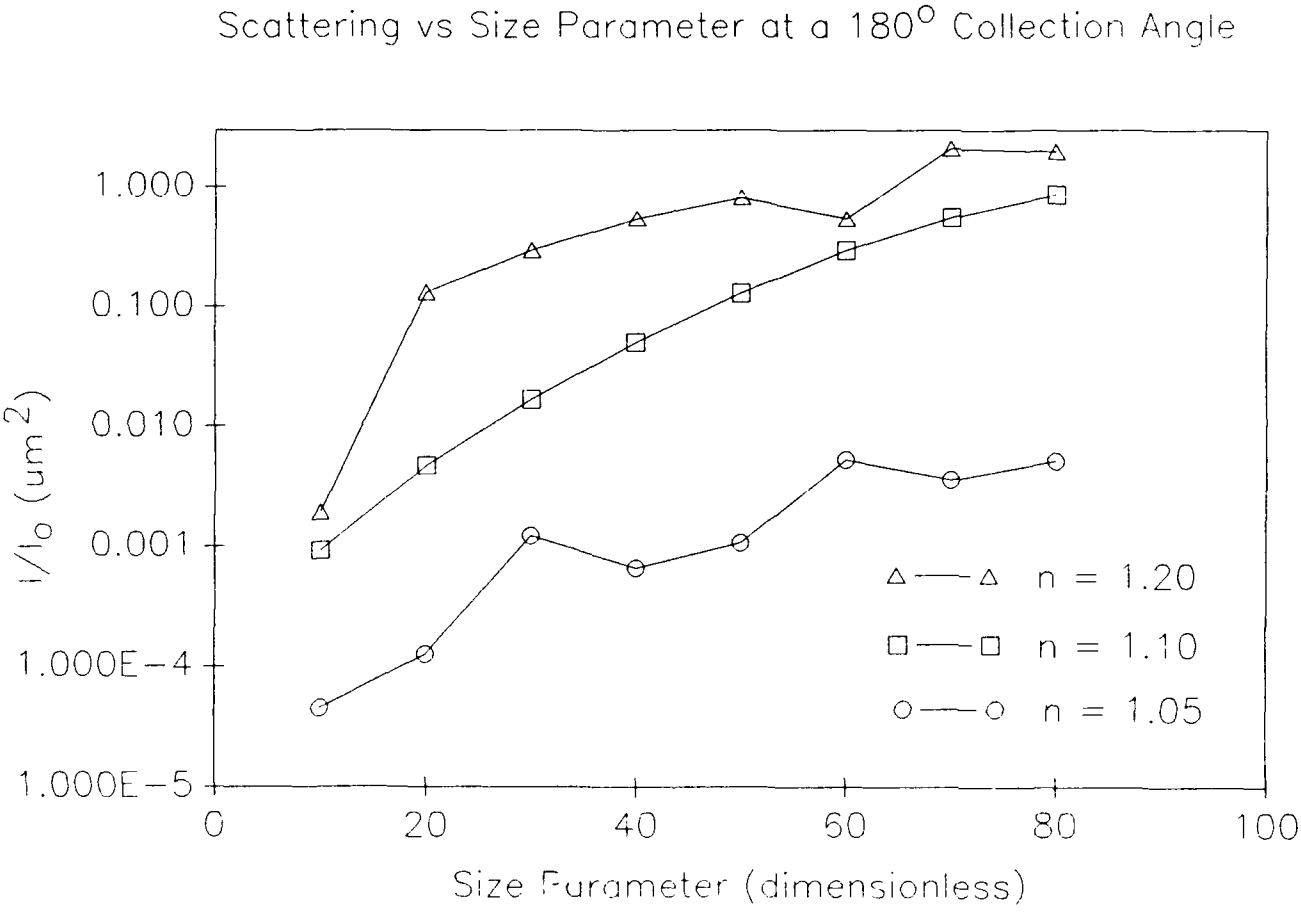

Figure 4. Mie scattering computations for particles with three indices of refraction collected at 180 degrees.

3. EXPERIMENTAL BREADBOARD

The key elements of the Phase I breadboard (see Figure 2) are:

* Laser diode Melles Griot model 06DLL707 with temperature compensation and power control.
* Three Bragg cells Isomet model 1205C-1 specially coated to cover the laser diode wavelength of 815 nm. The Bragg cells were powered by three separate drivers with corresponding constant frequencies of 75, 80, and 90 MHz. This choice of frequencies allowed for spectral separation of both the horizontal and vertical velocity components.
* Avalanche photodiode (APD) Texas Optoelectronics model TIED88 and custom made preamplifier board.
* Programmable digital signal processor (DSP).
* Optics to produce probe volume and collect the scattered light.

The laser diode operated TEM_{00} at 815 nm and was capable of providing 40 mw of power. For the purposes of Phase I the laser diode included a commercial temperature controller and power regulator which are bulky and not appropriate for an underwater system. However, these controllers would not be necessary in an ocean environment since the temperature of the ocean does not change by more than about 20 F in any particular location.

The laser beam was split into three beams and each was frequency shifted by one of the Bragg cells. These beams were crossed by a transmitting lens to form three overlapping fringe patterns which were spectrally separated. The difference in frequency between the two horizontal beams and the two vertical beams was 5 MHz and 10 MHz respectively. A parasitic diagonal shift of 15 MHz is also obtained but it was easily filtered out.

The APD is the optimum photodetector for near infrared detection. Its power requirement is much smaller than that required by a photomultiplier tube since its quantum efficiency is about ten times larger. Furthermore the APD is small and rugged. Unlike conventional laser Doppler velocimeters in which one detector is needed for each velocity component, a single detector was employed here to measure the vertical and horizontal velocity components. This is possible because the signals can be spectrally separated as explained above.

The programmable electronic processor was made by Signatec and included a Texas Instrument DSP320C25 which capable of 10^7 operations per second. Thus fast Fourier transforms can be performed in a few milliseconds. Furthermore, the processor could be programmed to perform any combination of algorithms for signal acquisition and processing. While the Phase I processor was hosted by an IBM personal computer, the Phase II version would stand alone.

The laser beam, which was nominally 8 mm in diameter, was minified to about 1 mm by a combination of two lenses (L_1 and L_2) with focal lengths of 200 and 25.4 mm. The beam splitter BS_1 separated the beam into two parts, a reflected part and a transmitted part. The transmitted portion of the beam was split again by BS_2. Each one of these three beams entered the respective Bragg cell. A combination of mirrors and lens L_3 was used to cross and focus the beams into a probe volume of about 60 μm in diameter and with vertical fringe spacing of about 25 μm, and horizontal fringe spacing of 28 μm. The light scattered by particles was collected at 160 degrees and focused on the APD by two lenses L_4 and L_5) with an equivalent F/2.5. The APD converted the scattered light into an electronic signal which was processed.

To demonstrate the three beam laser Doppler velocimeter in water, a Plexiglass test chamber was constructed. A pump flowed water through the chamber and a 2 mm orifice and valve were used to control the flow velocity. With the valve wide open the flow rate was measured to be 1.5 liters/min, corresponding to an average velocity at the 2 mm orifice of approximately 8 m/sec. Polystyrene particles with a diameter of 9.87 μm and monodisperse to within 0.057 μm were added to the water to provide calibrated scatterers to be measured by the LDV.

4. RESULTS

Signal amplitude and signal to noise ratio

The largest signals corresponded to particles traveling through the center of the Gaussian probe volume. The peak pedestal of these signals had values of about 200 mv. The amplitude of these signals could be predicted with the following expression:

Signal Amplitude = I_p x R,

where I_p represents the peak of the pedestal and is given in watts of collected light, and R is the detector response which is given in volts/watt.

I_p was estimated from the Mie scattering solution knowing the particle size (10 μm), the index of refraction (1.2), the angle of collection (160), the F# of collection (2.5), and the laser wavelength (815 nm). The scattering cross-section of a 10 micron polystyrene particle in water was thus computed to be about 0.14 μm^2 (see the value of I/Io on Table 1 for a 10.37 μm particle). The illuminating beams had a combined total power of 20 mw and focused to a 60 μm diameter probe volume. The power density in the middle of the probe volume was then estimated at 7×10^{-6} w/μm^2. The power density multiplied by the scattering cross-section yields the total collected light, which is 9.8×10^{-7} watts.

The response of the detector is given by:

R = R_e x APD gain x terminal resistance x amplifier gain.

For the APD at a wavelength of 815 nm, the radiant responsivity R_e = 0.3 amps/watt; the APD gain was calibrated to be 25, the terminal resistance was 1000 ohms, and the amplifier gain was 75. These values yield a detector response of 5.6×10^5 volts/watt.

The peak signal amplitude can then be computed to be 550 mv. The signal output was ac coupled which limited the peak signal to about 50% of its value, that is 275 mv. This prediction is very close to the measured value of 200 mv and gave us confidence to predict the signal level associated with particles of different diameter and index of refraction.

For the amplifier gain of 75 the peak to peak electronic noise was about 40 mv. This was established given that an ac threshold of 20 mv excluded triggering on the electronic noise. Since the measured signals had a peak amplitude of 200 mv, the signal to noise ratio was about 10. This signal to noise ratio could also be established from the frequency spectrum by comparing the height of the signal bins and the adjacent noise bins. It was desirable to set the threshold level above the electronic noise to avoid triggering on the noise and fill up the memory with useless information. Since this signal/noise corresponded to a scattering cross section of 0.14 μm^2, it could be concluded that the minimum scattering cross-section would be approximately 0.014 μm^2 for a signal to noise ratio of unity This minimum could be decreased by reducing the noise, and there are various ways to meet this goal. First, since the frequency range of interest was established to be between 1.1 and 5.5 MHz,

analog filters could be used to limit the frequency to this range. This would reduce the bandwidth to about 10 MHz instead of the 50 MHz used during Phase I. Second, more efficient APD and amplifier combinations could be selected. The combined effect of these two improvements would result in reducing the noise by about a factor of 10. Under these conditions the minimum scattering cross-section would be 0.0014 μm^2.

The scattering cross-section is a function of particle size and index of refraction. Tables 1 through 6 show sample computations obtained by solving the Mie scattering equations for indices of refraction 1.05, 1.1, and 1.2. These values are typical of the micro-organisms and sediment found in the ocean. If we use the value of 0.0014 μm^2 as the minimum scattering cross section detectable by the system, it can be seen from these tables that for an index of refraction of 1.2 the minimum detectable diameter is about 2 μm; for an index of refraction of 1.1 the minimum detectable diameter is about 5 μm, and for an index of refraction of 1.05 the minimum detectable diameter is about 12 μm.

The velocity distribution

Experiments were run at various flow rates and with the test chamber inclined at various angles to produce different velocity components in the horizontal and vertical directions. Figures 5 and 6 show the results of a sample burst corresponding to one of these experiments for an inclination of the test chamber of 34 degrees and the flow control valve wide open. The frequency spectrum was obtained by performing an FFT on the collected data. Notice the values of f_1 = 5.225 MHz and f_2 = 10.25 MHz. Substituting these values into equations (1) and (2), we arrive with velocity values of U = V = 6.2 m/s. In this particular example the U and V components are equal and correspond to flow moving at 45 degrees. In general, U and V can have arbitrary values. This arrangement permits the measurement of flow velocity and turbulence at arbitrary directions; including recirculating flows. Figure 7 shows a portion of the signal corresponding to a stationary particle (pump off). The Fourier transform of this signal is shown on Figure 8 and demonstrates that for the no flow case the measured frequency corresponds only to the Bragg cell frequency shift (i.e. 5 and 10 MHz respectively).

A sample of 13 bursts was analyze to study the turbulence of the flow coming out of the orifice. This is a very small sample for any statistical purposes but it serves to demonstrate a concept. The mean velocity of the flow at this point based on the 13 measurements was 8.76 m/sec. The direction of flow was found to be 56^{o}. The standard deviation of both the velocity and direction of the flow was found to be 10%, indicating the high degree of turbulence. A visual display of these measurements is shown on Figure 9.

PHASE II SYSTEM

For a maximum velocity of 10 m/s and assuming a fringe spacing of 25 microns we estimated above that the required frequency shifts would be 1.6, and 3.2 MHz. These could be achieved with three Bragg cells operating at 80, 81.6, and 84.8 MHz, or with two Bragg cells operating at 80 and 81.6 MHz while utilizing the first and second orders. Alternatively, these frequency shifts could be obtained by running three laser diodes at slightly different wavelengths. In Phase I we demonstrated that the three Bragg cell approach is sound; the two Bragg cell approach appears to be a straight forward extension. Here, two Bragg cells would be driven with frequencies of 80 MHz and 81.6 MHz, thus the second order frequencies would be 160 and 163.2 MHz. The horizontal velocity component could be measured by mixing the first order beams which yield a frequency shift of 1.6 MHz; the vertical component of the velocity could be measured by mixing the second order beams which yield a frequency shift of 3.2 MHz. It may also be worth considering the three laser approach in the beginning of Phase II since if they prove successful, they

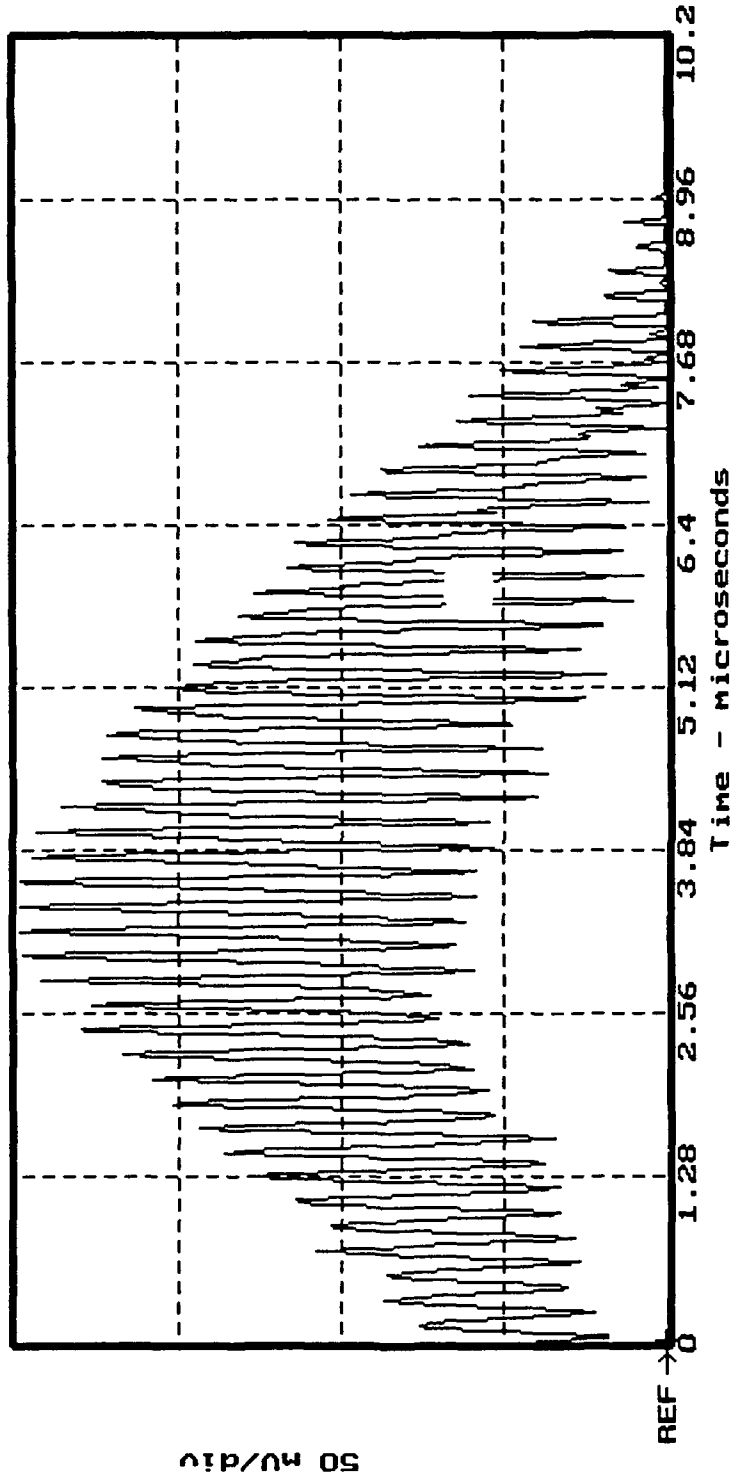

Figure 5. Time domain plot of a typical 10 μm polystyrene sphere with a velocity of 6.2 m/sec traveling at 45 degrees to the horizontal.

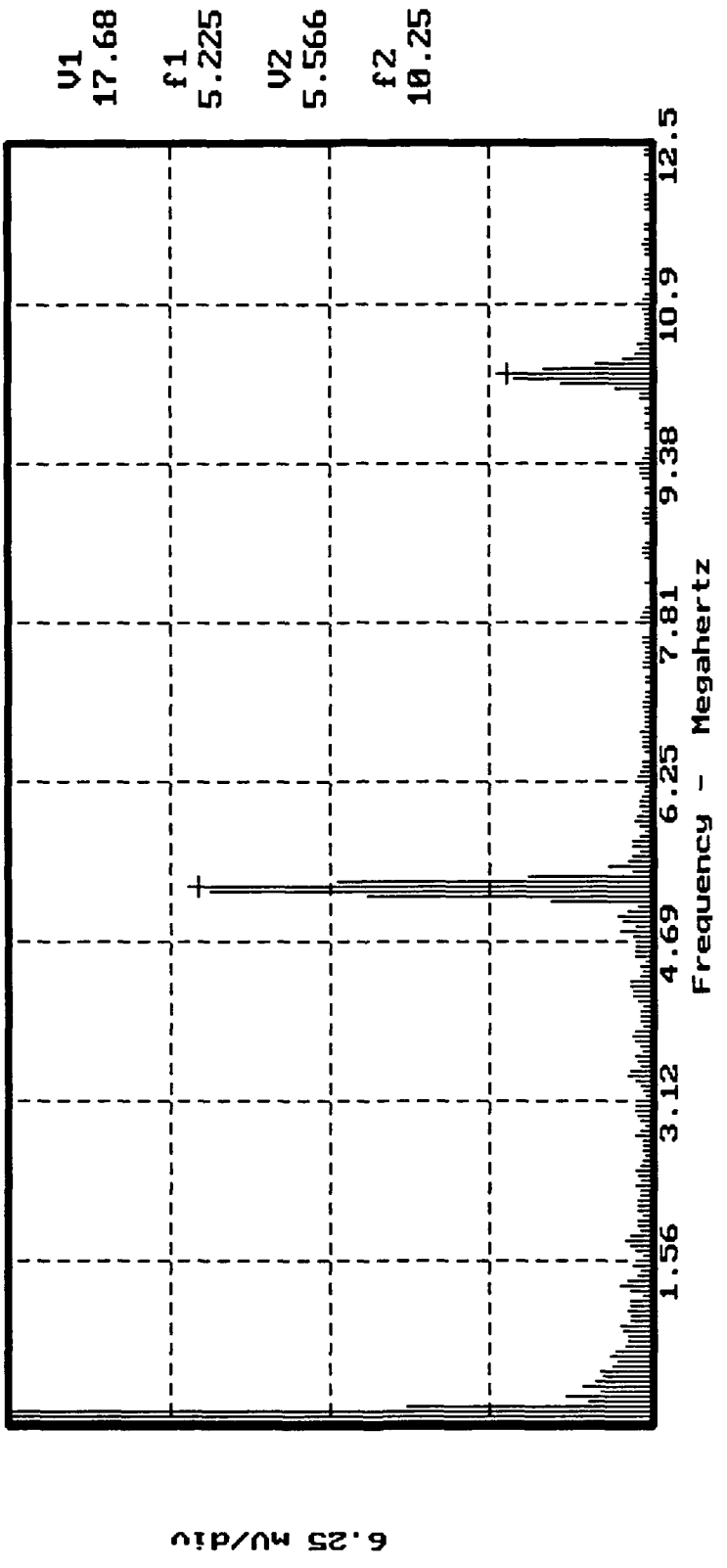

Figure 6. FFT of the particle signal shown in Figure 5.

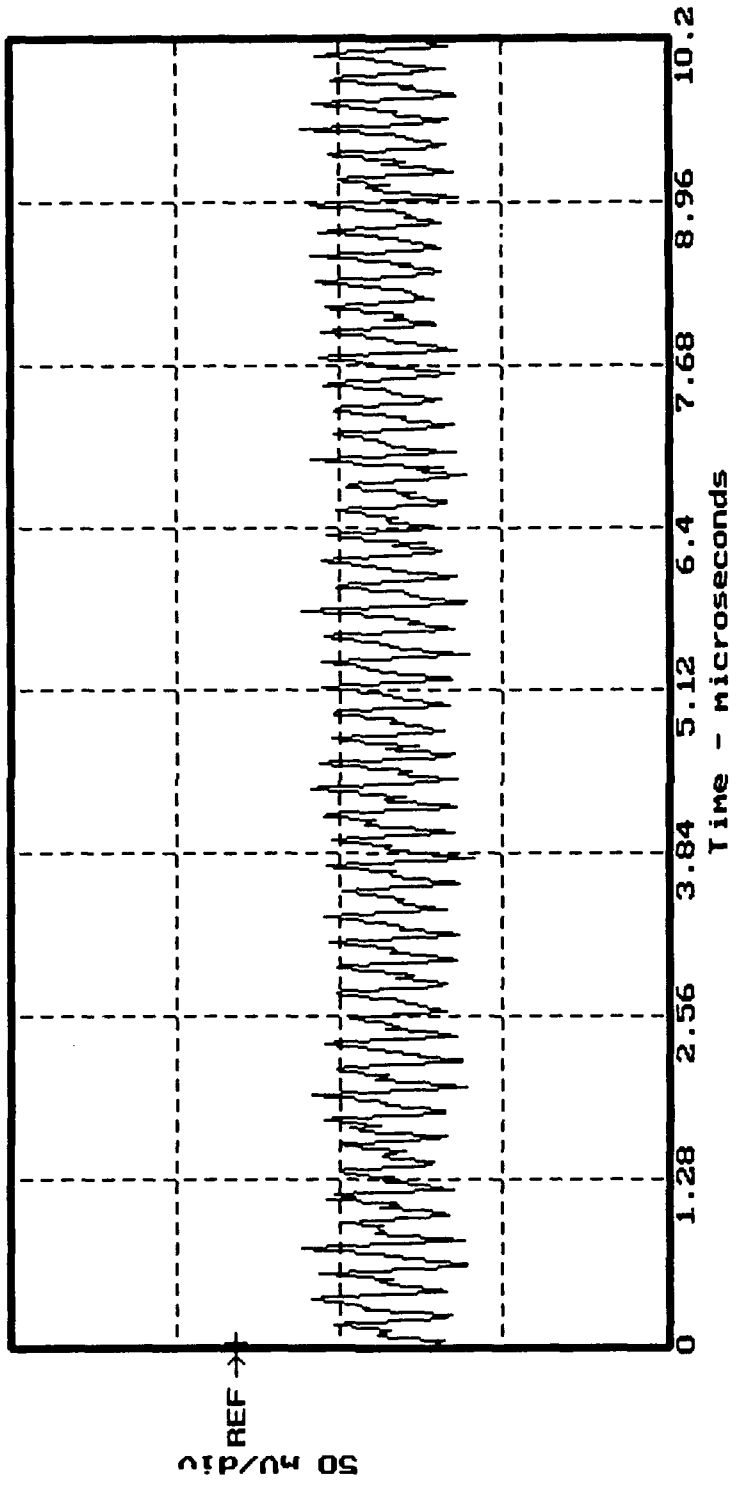

Figure 7. Time domain plot of a static, 10 μm diameter particle.

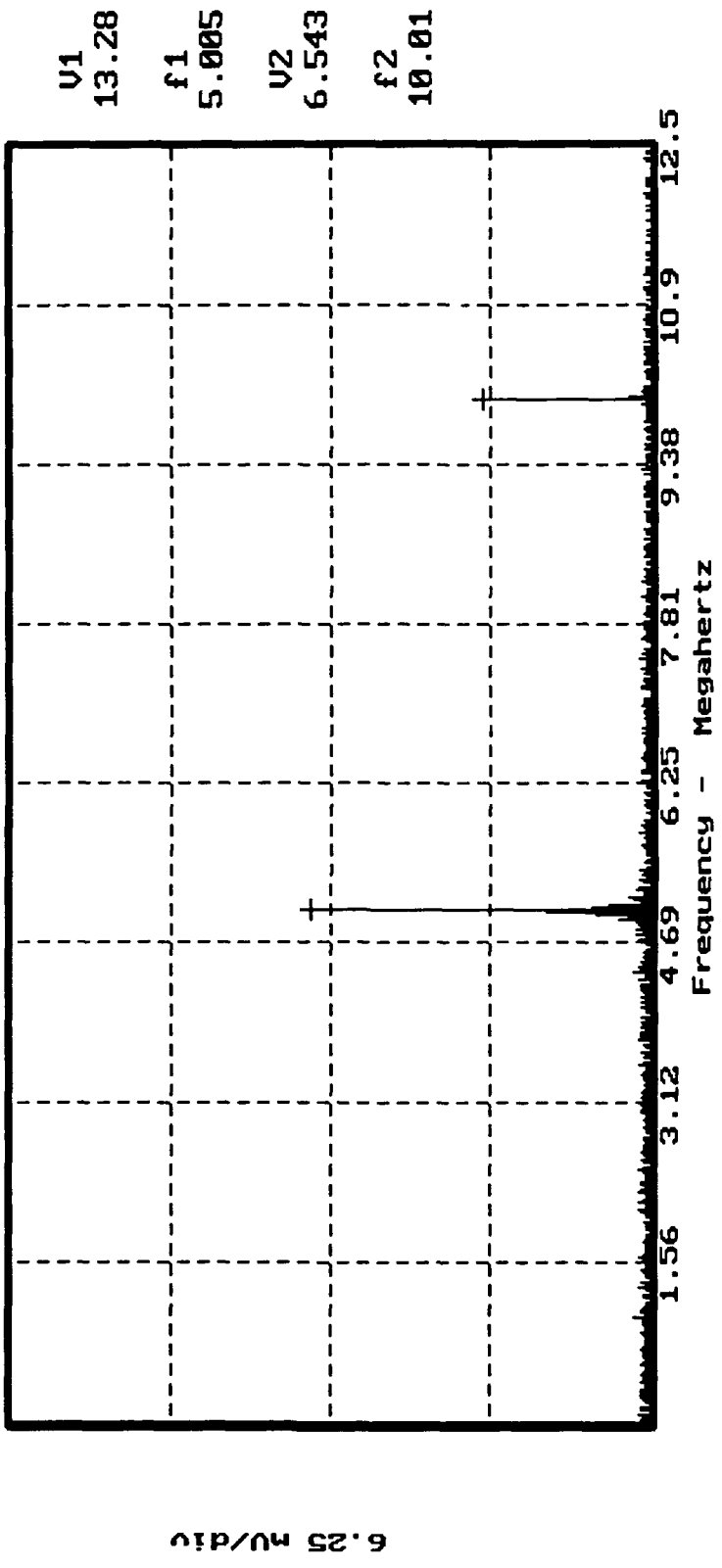

Figure 8. FFT of the static particle signal shown in Figure 7.

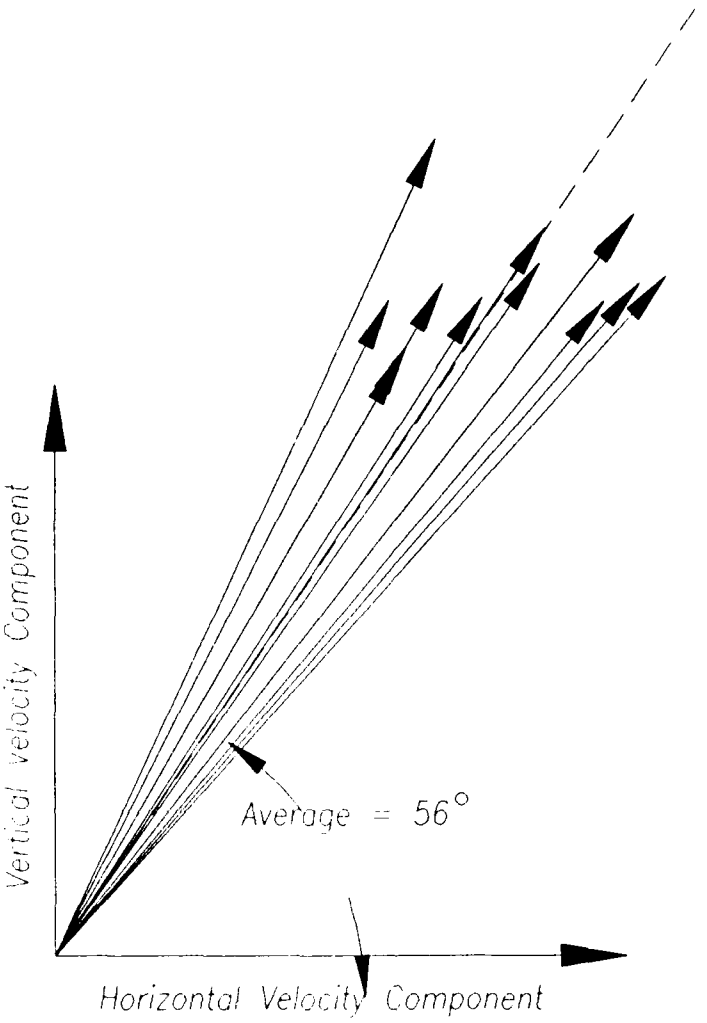

Figure 9. Scatter in velocity data.

consume less power than the Bragg cells. Since this approach has not been demonstrated, we will describe the Phase II system under the assumption that three Bragg cells will be used for frequency shifting.

The complete Phase II system is expected to measure 7" x 26" as indicated on Figure 10. The system will include a battery pack, the electronic processor, memory, laser power supply (this may or may not be necessary), Bragg cell drivers, single mode diode laser, telescope for beam conditioning, two beam splitters, three Bragg cells, three rhombs for beam steering, a plate beam splitter, transmitting lens, receiving lens, and avalanche photodiode. The shape of the system is expected to be cylindrical with a single window for transmitting the laser beams and receiving the backscattered light.

An alternative Phase II system is shown on Figure 11. This alternative system would incorporate particle sizing capability. Based on the discussion above, the beast result are expected when the light is collected in the forward scattering direction. Thus, this system would include a fiber optic receiver which collects the scattered light and transfers it to the photodetector. Furthermore, the probe volume may have to be shaped as an elongated sheet as indicated on Appendix A, to avoid the Gaussian ambiguity associated with a round beam. The final configuration will depend on the needed resolution. The alternative system will also include the capability of measuring the transmitted laser beam in order to correct the scattered signal by the obscuration.

Data acquisition and memory requirements.

The choice between solid state memory and a more permanent record, such as a tape, would have to be made during the Phase II effort. Solid state memory requires very little power to operate but it is vulnerable to power outage. A tape backup, or some other means of permanent memory may be necessary if the chances of power interruption are reasonably large. The information to be stored in memory consists of the mean and fluctuation of the horizontal and vertical velocity components, as well as the Reynolds stress and the time of collection. A total of six 2-byte parameters (U bar, V bar, U', V', U'V', t) are expected to be stored for each run. A run should consist of approximately 10,000 particles measured over 20 seconds or so every hour or as defined by a data collection logic. The time of collection or the data rate would have to be automatically adjusted to account for variations on the data rate. The raw data associated with 10,000 particles is about 1 Mb. To avoid a large electronic processor actual high speed memory will be limited to 64 Kb and the data will be acquired in 16 intervals. The information associated with these 10,000 particles will then be condensed to six 2-byte parameters for a total of 12 bytes.

Assuming that data are acquired every hour for six months, a total of 4320 runs will be stored which translates to 51840 bytes. Alternatively data may be acquired when prompted by an external sensor such as a microphone or an accelerometer. Under this last scenario data would be acquired when the conditions of the ocean exceed some pre-determined threshold.

Scale = 0.25

Enclosure Dimensions (Cylinder) 7" x 36"

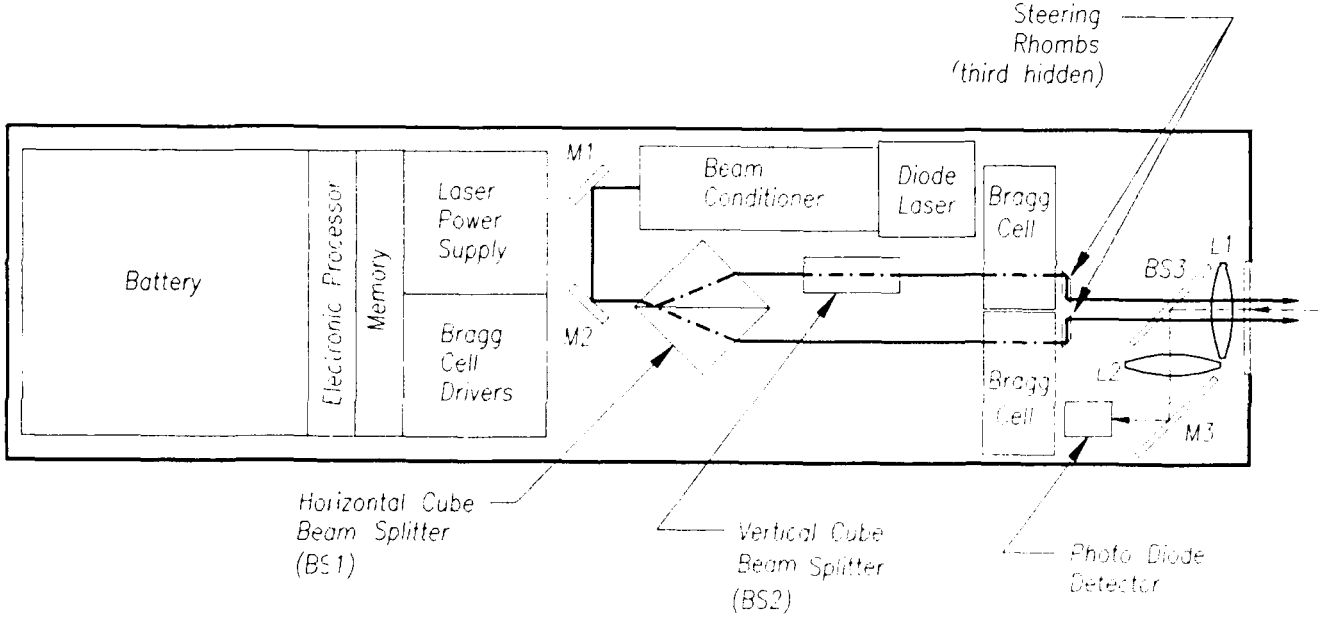

Figure 10. Scaled drawing of proposed Phase II LDV.

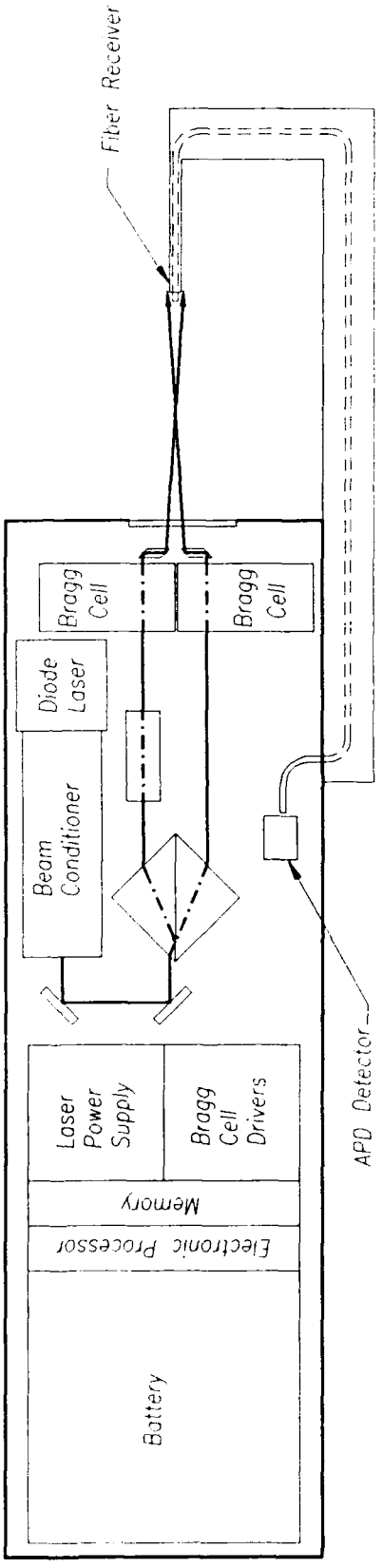

Figure 11. Alternative Phase III LDV system utilizing forward scattering via an optical fiber.

Power budget

20 MHz electronic processor with 64 Kb of memory	6 watts
Three Bragg cells	3 watts
40 mw laser diode	0.2 watts
APD	0.16 watts
External sensor (if chosen)	0.02 watts

The total power consumption would be about 10 watts during data acquisition, and about 0.02 watts during waiting periods.

For 24 events per day with a duration of 20 seconds the total data acquisition time for six months would be 24 hours. The waiting time would be 4296 hours. The total energy required by the system would then be:

24 hrs x 10 watts + 4296 hours x 0.02 watts = 326 watt-hours.

The system could be designed to operate at 12 volts thus requiring 27 amp-hours. There are several batteries which appear to satisfy this energy requirement while maintaining a reasonable size. Examples of these batteries include lead calcium and sealed lead acid. The precise choice of batteries will be an important task during Phase II.

CONCLUSIONS AND RECOMMENDATIONS

1. The programmable processor allows the implementation of intelligent algorithms which can be specifically tailored to optimize the data acquisition and processing in a marine environment.

2. The three Bragg cell concept allows for simple discrimination of two velocity components using a single wavelength laser and a single photodetector.

3. The diode laser provides ample power with very little energy consumption making it an ideal choice for a battery operated system.

4. Particle sizing can be added to the Phase I system with reasonably simple modifications. Forward scattering collection may be required to obtain adequate signal resolution.

To demonstrate the three beam LDV in water, a Plexiglass test chamber was constructed. A pump flowed water through the chamber and a 2 mm orifice and valve were used to control the flow velocity. With the valve wide open the flow rate was measured to be 1.5 liters/min, corresponding to an average velocity at the 2 mm orifice of approximately 8 m/sec. Polystyrene particles with a diameter of 9.87 μm and monodisperse to within 0.057 μm were added to the water to provide calibrated scatterers to be measured by the LDV. Two lenses were used to provide an F/2.5 collection system which focused the scattered light onto an APD detector. The signal from this detector was amplified and sent to the programmable DSP.

AIAA'84

AIAA-84-0203

A Technique Combining the Visibility of a Doppler Signal with the Peak Intensity of the Pedestal to Measure the Size and Velocity of Droplets in a Spray

C.F. Hess, Spectron Development Labs.,
Costa Mesa, CA

AIAA 22nd Aerospace Sciences Meeting

January 9-12, 1984/Reno, Nevada

A TECHNIQUE COMBINING THE VISIBILITY OF A DOPPLER SIGNAL WITH THE PEAK INTENSITY OF THE PEDESTAL TO MEASURE THE SIZE AND VELOCITY OF DROPLETS IN A SPRAY

Cecil F. Hess, Ph.D.
Spectron Development Laboratories, Inc.
Costa Mesa, California 92626

Abstract

A technique combining the visibility of a Doppler signal and the intensity of the scattered light to measure the size and velocity of particles is presented. It is shown that using only the visibility technique can lead to large errors under many conditions such as dense sprays. It is also shown that this error is considerably reduced and very high resolution is obtained by combining the visibility with the intensity of the scattered light. An instrument was developed using this new concept and measurements were performed in sprays of known characteristics. The results of monodispersed, bimodal and trimodal sprays are reported.

Introduction

The need for characterizing droplet environments (especially sprays) in many combustion processes is well established. Accurate spatially resolved measurements of the size, velocity and number density of the droplets, and the velocity of the gas are needed by system developers and modelers.

The ability to distinguish between droplet velocity and gas velocity is important since together with the droplet size it yields local Reynolds numbers from which particle drag coefficients can be determined.

In a combustion environment, the rate of evaporation of the droplets is determined by the rate of change of diameter of individual droplets. This quantitative information of the drop size and velocity distributions is needed throughout the spray as a function of space and time.

Techniques are, therefore, needed that can provide the above information nonintrusively, accurately and in real time from real sprays. There are several techniques that meet some of the conditions listed above. They can be grouped as imaging and scattering techniques. However, only a few of these techniques can be used for simultaneous measurement of size and velocity at a point. The two parameters used to date in these techniques are the visibility of a Doppler signal and the absolute intensity of the scattered light. This paper reports very recent research that shows the errors associated with the visibility technique, and a new method that uses simultaneously the visibility of the Doppler signal and the pedestal's peak intensity to perform a size measurement. This technique is referred to as Visibility/Intensity (V/I).

Results obtained with the V/I technique are reported for monodispersed, bimodal and trimodal sprays and monodispersed string of droplets. The mondispersed sprays offer great potential as calibration sources. The results show that by virtue of combining the visibility and intensity very precise measurements are possible in sprays and environments where visibility only will not perform.

Associated Research

The interferometric technique to measure the size and velocity of particles flowing in a fluid has been in existence for approximately one decade. Farmer[1] introduced the concept of using visibility for particle sizing in the forward scattering direction. Since then, many researchers have contributed to the development of the technique. Robinson and Chu[2], for instance, rederived Farmer's results using a more rigorous approach, and the definition of visibility through the first order Bessel function was confirmed experimentally in forward scatter. However, contrary to what was thought at the time, this visibility relationship could not be used at any angle other than the forward or zero degree. Adrian and Orloff[3] showed that the simple relationship valid in forward scattering could not be used in backscattering. This finding was also confirmed by Roberds[4], who in addition showed that the configuration of the receiving optics would also affect the relationship between visibility and size.

The biggest known limitation of the visibility technique was its inability to measure particles in a dense field. The main reason being that the probe volume when observed in the forward direction is big and, therefore, the criterion of single particle measurment is not always met. In addition, the technique dictated that the largest measurable droplet was of the order of the fringe spacing. This imposes a limitation of about 200 μm to the largest measurable particle and also results in a large probe volume, since a minimum number of fringes is needed (typically 8) to accurately process a Doppler signal.

Bachalo[5] formulated a mathematical model based on classical optics where the Mie scattering is approximated with refraction, diffraction and reflection. That model was used to predict the visibility of spherical particles in off-axis directions. Experimental results using monodispersed droplets confirmed the validity of the model under many conditions. Pendleton[6] later confirmed these results using a sophisticated numerical model that utilizes the full Mie equations. Recent work conducted by the author shows that there are two major limitations on the existing models. First, all the theories developed thus far predict the Mie scattering from beams of uniform intensity. Second, the formation of the fringe pattern at the probe volume may be affected by secondary scattering of particles immersed in the laser beams before they cross. As a result of these limitations, the relationship between visibility and size is not straightforward and considerable errors can be made. A model proposed by M. L. Yeoman et al[7] purports to eliminate the above problems. It neglects [illegible] interferometric [illegible]

the small one establishes a region of the big one where the hyperbolic variation of the visibility is negligible. Also digital analysis of the signals helps establish some that are in error. The research reported here shows that using the intensity of the pedestal of the scattered light in addition to the visibility will eliminate many of these errors, significantly improving measurement accuracy.

Errors in the Visibility Measurements

The prediction of the droplet size based on the visibility of the light scattered by the droplet crossing an interferometric pattern of fringes depends on the pattern itself. For a perfect system the fringe visibility should be 100% and the light scattered should be primarily of one type (refraction, reflection or diffraction). There are, however, many causes in practical environments that contribute to alter the fringe pattern and, therefore, confuse the relationship between visibility and size. The result is that apparent sizes instead of true sizes are often measured. As an example, droplets interacting with the laser beams before they cross will randomly reduce (or even destroy) the fringe visibility. If a droplet is measured at such time, it will appear bigger than its true size. There are several factors that produce an error in the visibility measurement and they are listed below. They are divided into two groups: the ones that reduce the visibility and the ones that increase it.

A) Factors that Reduce the Visibility

1) Particles prior to crossover destroy fringe contrast. This is a function of the spray density.

2) Beam excursions due to turbulent hot media.

3) Hyperboloidal reduction of visibility.

4) Light scattered by reflection/refraction can add destructively for large droplets immersed in a non-uniform (typically Gaussian) beam.

5) Multiple particles in probe volume.

6) Increase in signal background. Normally from many little drops present in the probe volume.

7) Loss of fringe contrast due to faulty components (beamsplitter, etc.)

B) Factors that Increase the Visibility

1) Out of focus drops "masked" by the pinhole.

2) High time rise on leading edge of signal.

The Visibility/Intensity (V/I) Technique

This technique makes use not only of the visibility of a Doppler signal but also the peak intensity of the pedestal. Both parameters are available in the signal and their cross-correlation can be used to eliminate faulty signals produced in many practical environments. This technique will especially prevent small particles (high visibility) from appearing as large. Figure 1 shows a Doppler trace where both the visibility and the peak intensity of the pedestal are indicated. There is a relationship between the size of the droplet and the amount of scattered light given by Mie theory. This relationship can be used to eliminate signals with an apparently different size by using the following logic: droplets that produce a certain visibility are associated with a given size; hence, they should scatter light with a given intensity (characterized by I_p). Two exceptions are contemplated: first, droplets with the correct visibility will scatter different amounts of light due to the Gaussian nature of the probe volume's intensity; second, droplets with an erroneous visibility will not scatter light with an intensity corresponding to their apparent size.

The V/I method will then establish intensity limits for every measured visibility. This will produce a well established probe volume as a function of size and will reject droplets measured with an erroneous visibility. For instance, assume that the size corresponding to a visibility V_1 is d_1. Then the light scattered will have a pedestal with maximum intensity $I_{p_1}(max)$. Since this intensity would only be detected from droplets crossing through the middle of the probe volume, Figure 1, more relaxing limits are proposed. That is I_{p_1} will be accepted when $I_{p_1}(min) \leq I_{p_1} \leq I_{p_1}(max)$. Obviously, the broader the limits, the larger the error that can be allowed with the visibility technique.

Figure 2 shows three cases that illustrate the correcting properties of the V/I method. Figure 2a shows a droplet of size d_1 with visibility V_1 and intensity I_{p_1}. Since this last one is within established limits, the signal is accepted as valid. Figure 2b shows the signal produced by a droplet of diameter d_2 but the visibility was reduced to V_1 due to fringe contrast reduction. Since the visibility is V_1, this signal would be interpreted as having a diameter d_1. However, the peak intensity of the pedestal I_{p_2} corresponds to its true size (d_2) which is smaller than $I_{p_1}(min)$ (to which it is compared). Therefore, the signal is rejected. Figure 2c shows the signal of another droplet of diameter d_2 but with correct visibility V_2 and corresponding pedestal I_{p_2}. This last one will also be accepted.

Since the intensity limits are functions of droplet size, a variable filter like the one shown on Figure 3 is necessary. It contains the intensity limits $I_p(min)$, $I_p(max)$ corresponding to any visibility V. Figures 4a and 4b show the raw data and software filtered data of an intensity/visibility plot. Figure 4a shows that the intensity is bounded by $I_p(max)$ (with a few exceptions due to light reradiated by upstream droplets). Points with different intensity/visibility combinations can be either due to droplets moving through the edge of the Gaussian intensity profile of the probe volume or to droplets with an erroneous visibility. By limiting the intensity of the pedestal for which a signal is considered valid, two things are accomplished: (1) the limits of the probe volume are carefully established; and, (2) most importantly, most of the signals with erroneous visibility are rejected.

Results

Experimental results are presented to illustrate the accuracy and resolution of the visibility/intensity technique, and how it compares with visibility only.

Effect of Beam Blockage on Size Distribution

The effect of a very dense spray blocking the laser beams before the probe volume was studied. Figure 5a shows the histogram produced when monodispersed droplets travel through the middle of an undisturbed probe volume. Figure 5b shows a histogram obtained with the visibility technique of the same monodispersed droplets but now the laser beams have traveled through a real spray before crossing. We made sure that the spray was not going into the probe volume. The fringe pattern produced by crossing two laser beams is well behaved and theoretically predicted in the undisturbed case. However, when the beams travel through a spray, this fringe pattern can be considerably altered due to random beam blockage. The result can be a distorted Doppler signal with a visibility, both lower and higher than that predicted theoretically. Considerable error in the size distribution will then be observed. The size of the error depends on the visibility itself. It is quite apparent from the histograms that what should be a monodispersed distribution is measured as a very broad one. The next histogram shown on Figure 5c shows the results obtained with V'I when the beams travel through the spray before crossing (same conditions as Figure 5b). Notice that a very narrow distribution is thus obtained.

Measurements with the Berglund Liu Droplet Generator

The calibration and verification source used in these experiments was the Berglund Liu monodisperse droplet generator. This generator can work in two modes: (a) it can generate a string of droplets of known size and equally spaced at the measurement point; (b) using a cap and dispersion air, these droplets can be dispersed into a spray of monodispersed droplets.

It has been observed in previous studies[8] that under some dispersion air conditions, some of the droplets will collide and form other droplets with double or even triple the volume. Therefore, if the primary droplet diameter is d_0, droplets with diameter $2^{1/3} d_0$ and $3^{1/3} d_0$ can be produced. It must be pointed out that in these studies, we did not obtain photographic measurements to verify the presence of the secondary droplets. The size of the primary droplets was accurately predicted from the flow rate and frequency of vibration of the pinhole.

One limitation imposed by the Berglund Liu is that it cannot produce droplets of a given size at arbitrary spacing. Since the measurement instrument requires the presence of only one droplet in the probe volume, that limits the size droplet that can be measured.

The procedure used in these experiments was to produce a string of large monodispersed droplets to calibrate the instrument. Then smaller droplets were produced by increasing the frequency of vibration of the orifice, and with the dispersion air a spray of these droplets was formed. Typical number density at the probe volume was 500 droplets/cm^3 and the diameter of the spray at the plane of measurements was about 4 mm.

A DSI system with V'I capability was used to obtain the data shown below.

Optical configuration:

- Collection angle of 30°
- Transmitting lens = 495 mm
- Waist diameter = 300 μm
- Fringe spacing = 13.6 μm
- Collection F# = 5

The high voltage to the photomultiplier was established with a droplet string of diameter 150 μm.

The size range of interest was 9 to 92 μm.

A spray of droplets with primary diameter of 53 μm was then produced using the Berglund Liu with a flow rate of 0.21 cc/min and frequency of 45.88 Hz and the dispersion air. For the conditions selected above, this size will produce a visibility of 58%.

Notice that for primary droplets of 53 μm, the doublets will have a diameter of $2^{1/3} \times 53$ = 66 μm, and the triplets' diameter will be $3^{1/3} \times 53$ = 76 μm.

Results are shown for both Visibility/Intensity and visibility only to provide some comparison.

Figure 6 shows the measurements of the monodispersed spray of 53 μm.

Figure 7a shows the data of the spray formed of primary droplets and doublets.

Figure 7b shows results similar to Figure 7a but obtained with visibility only. Notice how much broader the distributions are.

Figure 7c shows a spray containing primary droplets, doublets and triplets.

Figure 7d shows results similar to Figure 7c but obtained with visibility only. Notice that the distribution is broader and the resolution is not as fine.

Both the accuracy and resolution of these measurements are very good. The theoretically predicted sizes are 53 μm, 66 μm, and 76 μm. The corresponding measured diameters are (52 to 54), (63 to 65), and 73 μm.

Larger errors (about 5%) can be expected when measuring the size at a higher visibility (80%).

Conclusions

The simultaneous measurement of visibility and intensity to measure and validate the diameter of droplets in a spray is shown to be accurate and with high resolution. This technique will extend the use of the present visibility technique to more realistic environments and will avoid

erroneous data by being selective during the data validation process. Additional work is, however, needed to establish the characteristics of the rejected data.

Since many of the erroneous data are the result of high droplet concentration, the percent of signals rejected can be used to establish the limits of the technique.

An automatic calibration logic used to establish the gain of the photodetector makes the technique self-calibrating.

Acknowledgements

This work was supported by the Combustion Fundamentals Section of NASA Lewis under Contract No. NAS3-23538, and the Air Force Office of Scientific Research (AFOSR) under contract No. F49620-83-C-0069.

The author is also greatful for the technical contributions of Dr. Anthony Smart and Mr. Tom Hunt.

References

1. W. M. Farmer, "Measurement of Particle Size, Number Density, and Velocity Using a Laser Interferometer", Applied Optics, Vol. 11, No. 11, (1972).

2. D. M. Robinson and W. P. Chu, Applied Optics, Vol. 14, 2177 (1975).

3. R. T. Adrian and K. L. Orloff, "Laser Anemometer Signals: Visibility Characteristics and Application to Particle Sizing", Applied Optics, Vol. 16, No. 3 (1977).

4. D. W. Roberds, "Particle Sizing Using Laser Interferometry", Applied Optics, Vol. 16, No. 7 (1976).

5. W. D. Bachalo, "Method for Measuring the Size and Velocity of Spheres by Dual-Beam Light Scatter Interferometry", Applied Optics, Vol. 19, No. 3 (1980).

6. J. D. Pendleton, "Mie and Refraction Theory Comparison for Particle Sizing with the Laser Velocimeter", Applied Optics, Vol. 21, No. 4. (1982).

7. M. L. Yeoman, H. J. White, B. J. Azzopadi, C. J. Bates, and P. J. Roberts, "Optical Development and Application of a Two Colour LDA System for the Simultaneous Measurement of Particle Size and Particle Velocity", Presented in the Winter Annual Meeting of ASME, Engineering Applications of Laser Velocimetry, Phoenix, Arizona, November 14-19 (1982).

8. B. H. Liu, R. N. Berglund, J. K. Argawal, "Experimental Studies of Optical Partile Counters", Atmospheric Environment, Vol. 8, pp. 717-732 (1974).

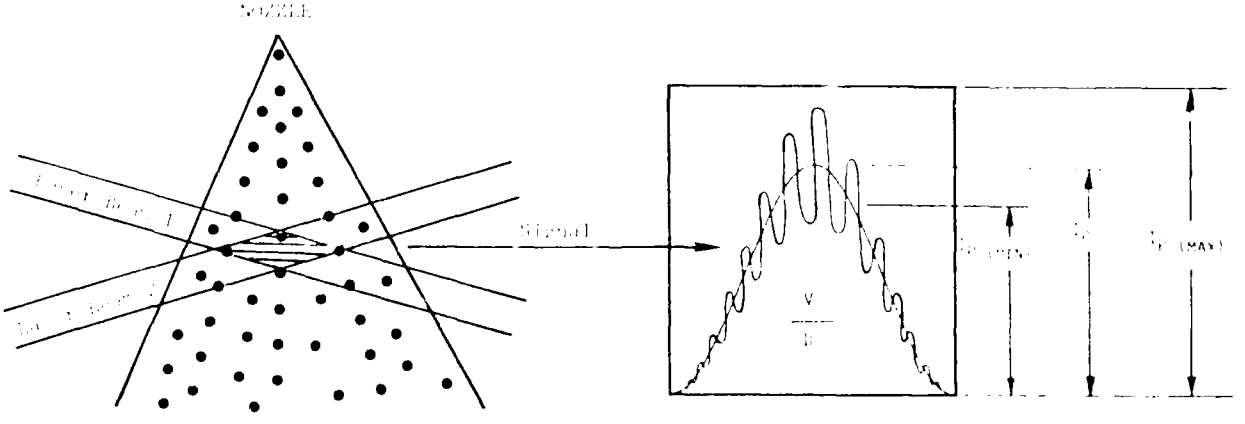

(a) (b)

Figure 1. [illegible] Doppler Burst Used in the Visibility Technique.

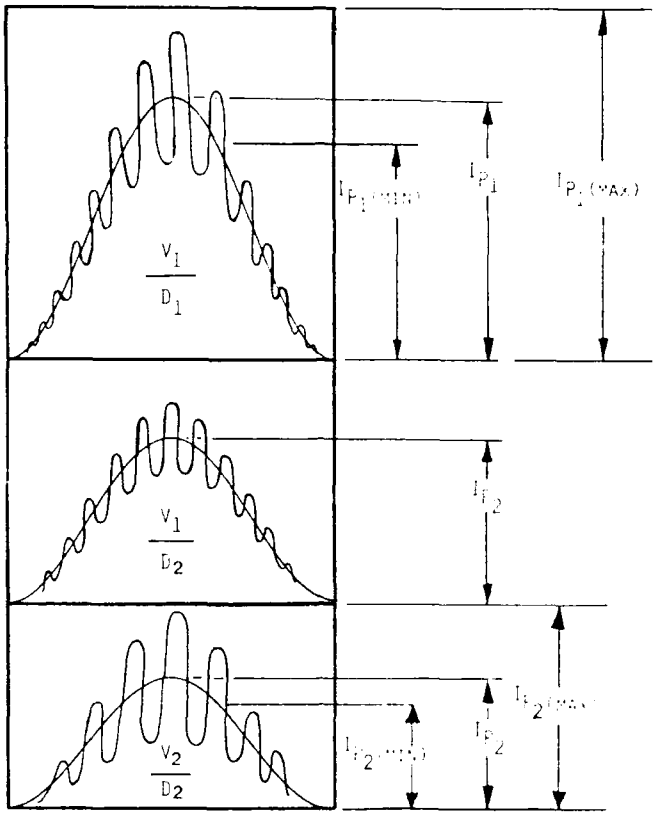

Figure 2. Visibility and Intensity of Two Size Droplets.

2(a) and 2(c) correspond to droplets traveling through the middle of an undisturbed probe volume; 2(b) could be from a small droplet traveling through the middle of a disturbed probe volume or a large droplet traveling through the edge of the Gaussian probe volume.

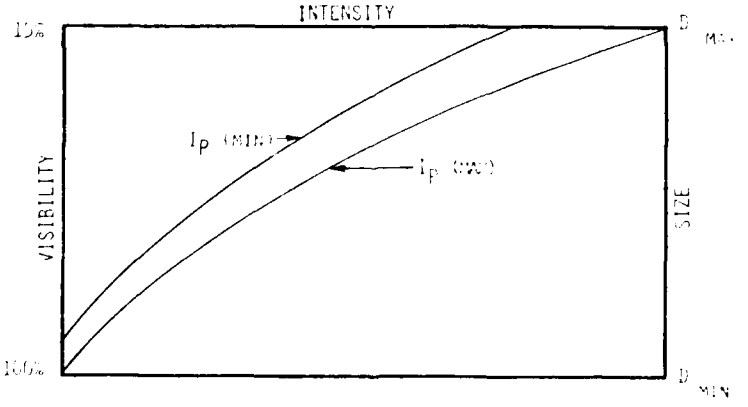

Figure 3. Variable Intensity vs. Visibility Software Filter

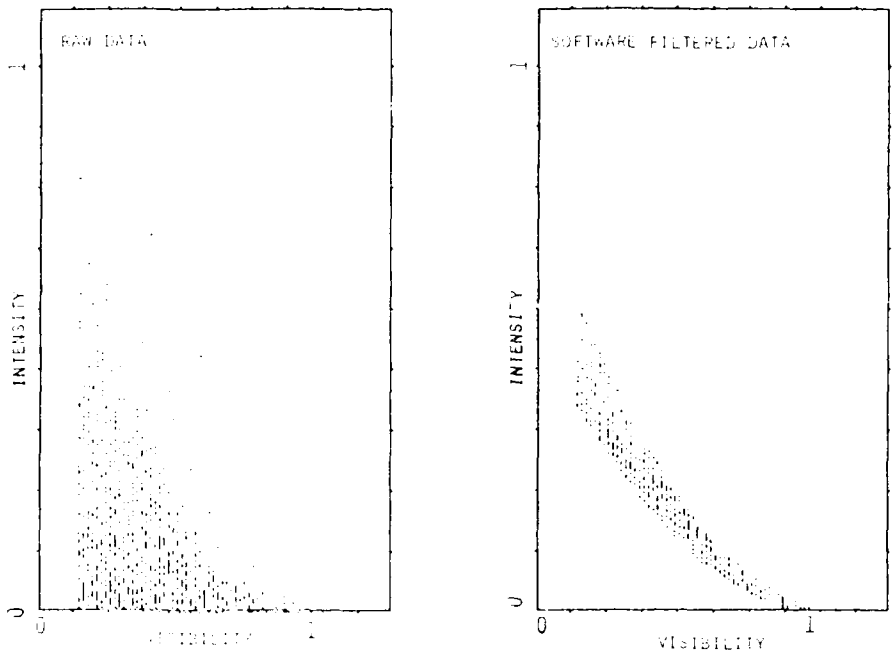

Figure 4. Visibility/Intensity Data of a Spray

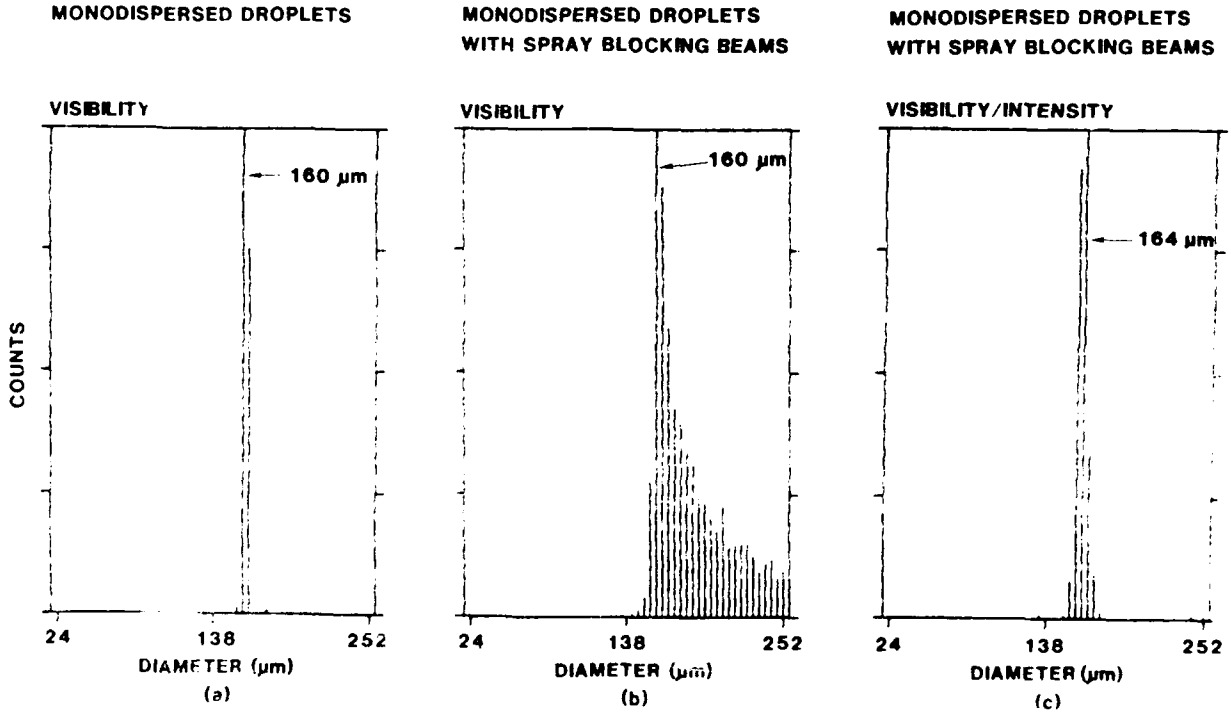

FRINGE SPACE = 37 μm
f No. = 5
θ = 30°

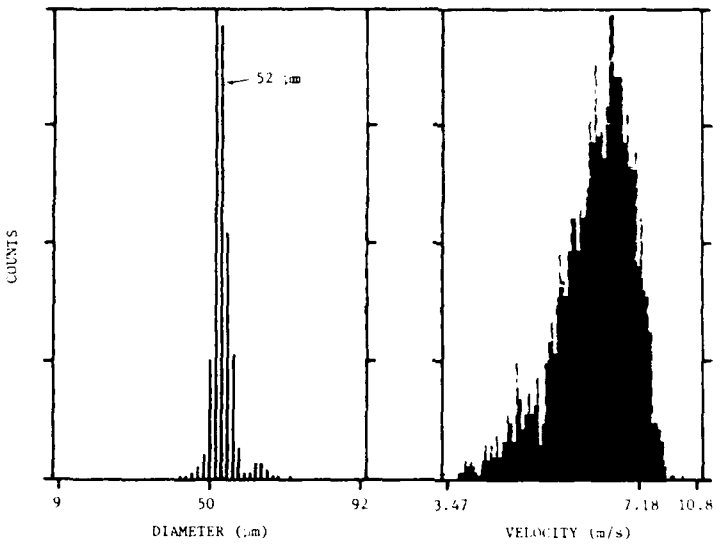

Figure 6. Visibility/Intensity Measurements of Monodispersed Spray

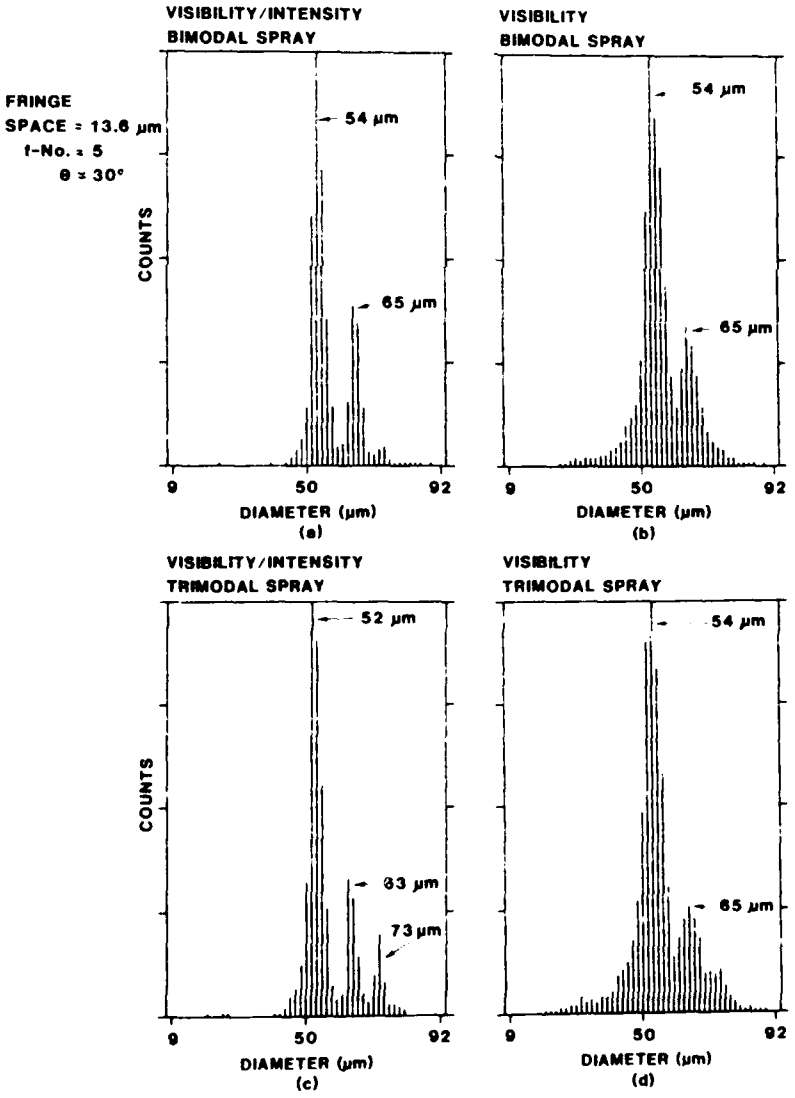

Figure 7. Size Distributions of Bimodal and Trimodal Sprays with Visibility and Visibility/Intensity

AIAA-85-1254

Laser Plane Velocimeter Technique for Particle Sizing and Velocity Measurement Applied to Rocket Plume Diagnostics

F. Li and C. F. Hess, Spectron Development Labs., Inc., Costa Mesa, CA

AIAA/SAE/ASME/ASEE 21st Joint Propulsion Conference

July 8-10, 1985 / Monterey California

LASER PLANE VELOCIMETER TECHNIQUE FOR PARTICLE SIZING AND VELOCITY MEASUREMENT APPLIED TO ROCKET PLUME DIAGNOSTICS

Funming Li, Scientist
and
Cecil F. Hess, Senior Scientist

Spectron Development Laboratories, Inc.
Costa Mesa, California 92626

Abstract

A nonintrusive particle sizing technique for measuring the size and velocity of particulates in a rocket plume is presented. This technique utilizes two crossing plane laser sheets to form an elongated probe volume with a known intensity profile. This shape of probe volume is not only less susceptible to beam wander, but also has the capability of two dimensional probing of particle size and velocity. Experimental results are presented for particles in the size range of 1.1 μm to 3.3 μm. These results show good consistency with Mie calculations. Actual measurements on rocket engine plumes would require a more powerful laser and faster electronic processors.

Introduction

The mechanism of particle formation in the combustor and plume of a rocket engine is not well understood.[1] These particulates can cause nozzle erosion resulting in performance degradation. A tungsten-tipped ablatively cooled sampling probe, immersed in a high-temperature (~4000K) environment with a large concentration of high-velocity aluminum oxide particles from the rocket motor exhaust, revealed that the solid particulates of Al_2O_3 were of submicron size and formed agglomerates of up to a few microns.[1] Thus, the ability to measure small particles (submicron) moving at high speed ($\sim 10^3$ m/s) in an optically noisy environment is the key to rocket engine research and performance assessment.

A laser plane velocimetry technique is presented in this paper. It is based on laser Doppler velocimetry, but laser beams are expanded into plane sheets which cross to form an elongated probe volume. Parametric numerical calculations of the Mie scattering solution were performed to establish the optical conditions less subject to error and ambiguity. An optical breadboard was built based on the results of the above studies. This breadboard was interfaced to an electronic data processor and a data management system.

Known size polystyrene microspheres were used to calibrate the system. Arbitrary distributions were formed by mixing different size polystyrene particles. Results are presented for monodisperse, bimodal and trimodal distributions. A Berglund-Liu droplet generator which is capable of producing strings of known size droplets[2] (>40μm) was also used. Smaller size particles were simulated by masking the receiver. This method was primarily used to align the optics and estimate the signal to noise ratio. Studies of the signal to noise ratio as a function of particle size at various photomultiplier gains showed that a higher power laser would be required to extend the measurable range to smaller size particles. For an actual rocket engine plume measurement, a faster electronic processor would also be needed.

Background

For particles significantly larger than the wavelength most of the light is scattered into the forward direction. The Fraunhofer diffraction theory adequately describes this scattering phenomenon.[3] There are several particle sizing techniques based on this principle. Swithenbank et al[4] utilized a monolithic photodiode array detector to analyze the spatial distribution of the scattered light. They then obtained the size distribution parameters form from the Fourier transform of the signal amplitude distributions. For particles in the size range of interest, the scattering function is a very complex function of the size, shape, index of refraction of the particle and the scattered angle.[3] The scattered light of large particles can be described by three components; namely, reflection, refraction and diffraction. The first two components are sensitive functions of the above parameters. On the other hand, the diffracted light intensity is independent of the refractive index and monotonically increases with size. Since the diffraction pattern of the scattered light is concentrated in the forward direction, it leads to a useful concept for particle sizing. The intensity of the scattered light collected in the forward direction will be insensitive to the variation of the refractive index and particle shape and be a monotonically increasing function of particle size. However, a forward scatter geometry implies a very large measurable volume. Moreover, beam stops are required to block the unscattered laser beams which can generate noise to the receiver. A reasonable compromise would be a near forward scattered angle of collection to avoid the incident laser beams, and reduce the size of the probe volume. It should be noted that for the size range of interest in rocket plumes (0.5 μm to 10 μm), Fraunhofer diffraction cannot be used. However, we found by solving the rigorous Mie scattering equations that many of the desirable features of the forward scattered light were also encountered at that size range.

Several optical scattering techniques have been proposed for measuring particle size and velocity. Very few, however, would work in a rocket plume environment. The visibility technique[5], for instance, is only applicable to particles much larger than the wavelength and, as was pointed out[6], beam degradation will introduce very large errors. The intensity ratioing technique[7] has been applied to small particles in a more limited size range (.3 μm to 2 μm).

IMAX/PMAX[8] which use three laser beams crossing at the probe volume are capable of measuring particles in the size range of interest. However, it is expected that at the rocket engine nozzle expansion region, large temperature gradients could cause beam wander which will limit the usability of these techniques. A technique

based on the scattered light intensity has demonstrated capability of measuring particle size distributions in the 1-30 μm range in a flow of high temperature.[9] We extend this method to a plane laser Doppler velocimetry type of measurement where particles are illuminated with a known light intensity. Particle sizes can be obtained from the scattered light intensity compared to Mie calculations. This method requires a known size particle to calibrate the system.

Description of Technique

In this technique, laser sheets are formed with cylindrical lenses and crossed to form a probe volume (Figure 1). This produces an elongated probe volume which provides the potential of measuring various positions of the plume at the same time. The size of the particles is obtained from the light scattered when they cross the probe volume, and the velocity, from the Doppler frequency. Because the probe volume is elongated, the intensity distribution is a very "flat" Gaussian, and we can think of the probe volume as a series of regions, each one with uniform, although different, intensities. Each one of these regions can be imaged to a photodetector, thus providing a simultaneous measurement of the particle size and velocity at different parts of the spray.

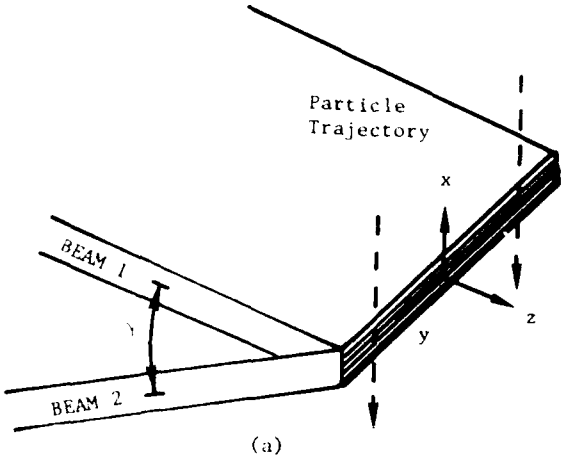

(a)

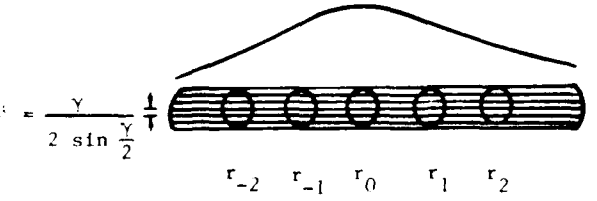

(b)

Fig. 1(a) Expanded laser sheets of wavelength λ crossing at angle γ to form an elongated probe volume. Particles move along x as shown.

(b) Light intensity at each portion of the probe volume $r_0, r_1 \ldots$ is known from the elongated Gaussian profile. Particle size can be determined from the light scattered from each portion of the probe volume. δ is the fringe spacing.

This is best illustrated with the mathematical expressions that define the above concept. The intensity of the light scattered by a particle of size $\alpha = \frac{\pi d}{\lambda}$, index of refraction n, at an angle θ is given by:

$$I_s = 2I_o K(\alpha,n,\theta) \exp\left[-2\left(\frac{x^2}{b_0^2} + \frac{y^2}{b_1^2} + \frac{z^2\gamma^2}{4b_0^2}\right)\right]$$

$$\left[\cosh\left(\frac{2xz\gamma}{b_0^2}\right) + \cos\frac{4\pi x \sin(\frac{\gamma}{2})}{\lambda} V\right], \qquad (1)$$

where d is the particle diameter, V is its visibility, λ the wavelength, K the scattering coefficient, γ the cross-section angle, b_0 the waist radius in the x direction, b_1 the waist radius in the y direction, and x,y,z the coordinates. Origin is defined at the center of the probe volume.

The scattering coefficient $K(\alpha,n,\theta)$ is, in general, a very complex function when d is of the order of λ. However, a parametric study, discussed later, showed that for shallow angles ($\theta < 5°$) the function is close to monotonic with particle size thus allowing the measurement of α. The particle size is obtained from the peak of the scattered light after the ac modulation is filtered out. This function is normally referred to as pedestal, and is given by

$$P_s = 2I_o K(\alpha,n,\theta) \exp\left[-2\left(\frac{x^2}{b_0^2} + \frac{y^2}{b_1^2} + \frac{z^2\gamma^2}{4b_0^2}\right)\right]$$

$$\left[\cosh\left(\frac{2xz\gamma}{b_0^2}\right)\right]. \qquad (2)$$

The peak of the scattered light for particles traveling in the x direction occurs at x = 0. Also the variation of the intensity in the z direction can be normally neglected. Therefore, the peak of the pedestal at any location y is given by

$$P_{max}(y) = 2I_o K(\alpha,n,\theta) \exp\left[-\frac{2y^2}{b_1^2}\right]. \qquad (3)$$

Since the laser beams are expanded in the y direction by cylindrical lenses, b_1 can be quite large (typically $b_1 \approx 20\, b_0$). The probe volume can then be divided into various segments of width Δy, such that each one of these segments has an associated value of y and for all practical purposes the intensity within any such segment is constant. Therefore,

$$P_{max}(y_i) = 2I_o K(\alpha,n,\theta) \exp\left[-\frac{2(i\Delta y)^2}{b_1^2}\right] \qquad (4)$$

Here i represents the segment number which might also correspond to an associated photodetector.

Each of these photodetectors will measure $P_{max}(y_i)$, and knowing i and Δy one can solve for $K(\alpha,n,\theta)$. For known values of θ and n one can then solve for the size parameter $\alpha = \frac{\pi d}{\lambda}$ and from it obtain the diameter of the particle.

Analytical Computations of the Scattering Functions

To obtain the size parameter α it is necessary to know the functional relationship of $K(\alpha,n,\theta)$ as given by Equation (4). As mentioned earlier, this function can be quite complex and it is necessary to find the conditions under which the ambiguities, if any, are within tolerable error margins. The computations were made using a modified version of Dave's[10] subroutines programmed in a PDP11 computer. Extensive parametric studies were conducted to establish optimum experimental conditions. These parameters include the angle of collection (θ). The solid angle of collection (Ω) and index of refraction ($n_1 - in_2$). The results show that near forward scattering angles of collection ($\theta \leq 5°$) offer the best optical characteristics.

Since the index of refraction of Al_2O_3 may vary with temperature[11] and particles of other materials and index of refraction may be present in the rocket plumes, it is important to establish conditions which are less sensitive to these variations. Both real (n_1) and imaginary (n_2) parts of the refractive indices have been varied to check the sensitivity of these parameters. The values were obtained from the document AFRPL-TR-81-54. Figures 2 and 3 show the scattered intensity as a function of the particle size parameter α for different values of n_1 and n_2 at different scattered angles. Figure 4 shows an integrated scattered intensity for a F/5.6 collection lens centered at different scattered angles.

It can be concluded from these calculations that the scattered light intensity will not be a sensitive function of the refractive index as long as the measurements are confined to shallow angles of collection ($\leq 5°$). In addition, a small uncertainty in n_1 will have little effect on the overall intensity function. For Al_2O_3 this change[11]

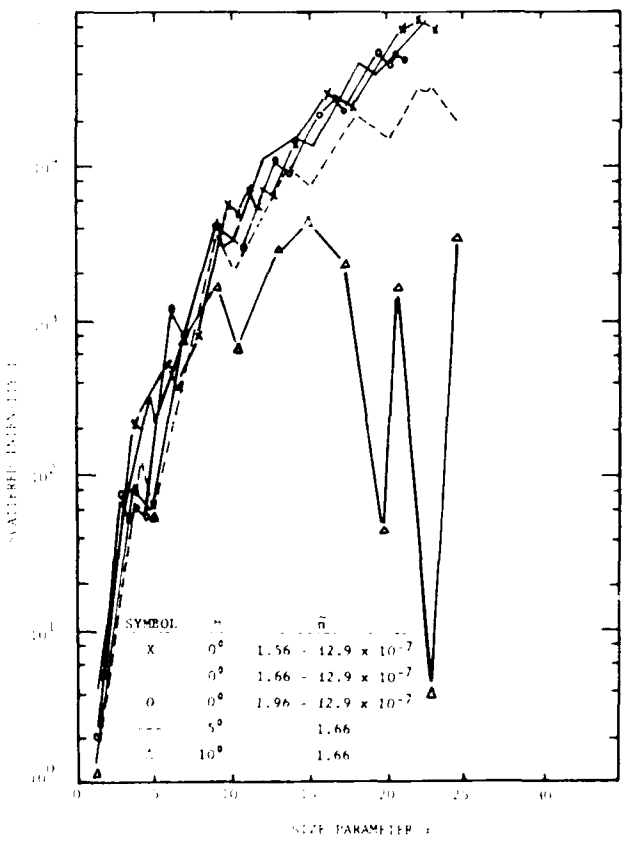

Fig. 2 Perpendicularly polarized scattered light intensity as a function of the size parameter α.

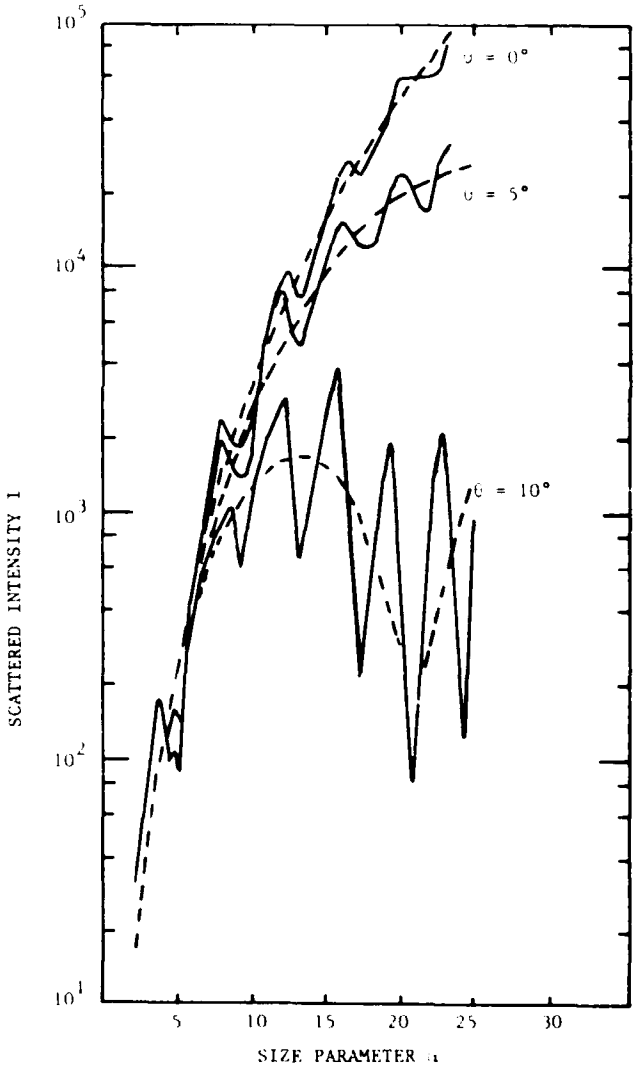

Fig. 3 Perpendicularly polarized scattered light intensity as a function of the size parameter α for different refractive indices (——$\hat{n}$ = 1.75, ----$\hat{n}$ = 1.75 - 10.29) at angles 0°, 5° and 10°.

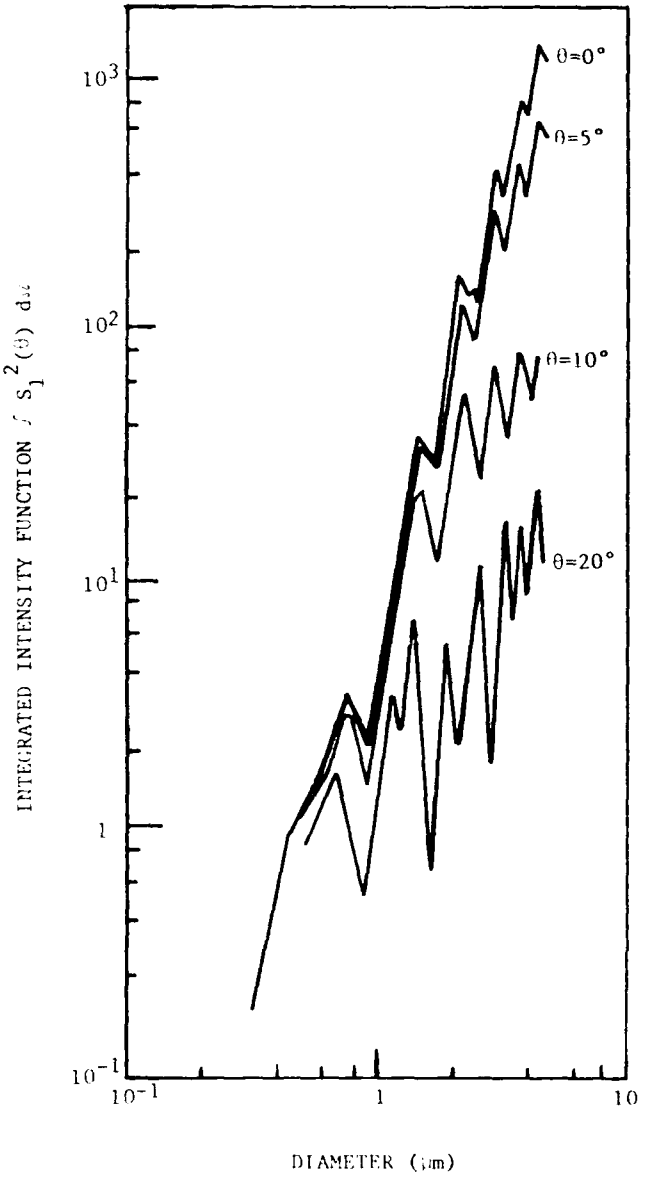

Fig. 4 Integrated intensity function for a collection lens F/5.6 and relative index of refraction $\tilde{n} = 1.81 - i1.15 \times 10^{-3}$ at $\theta = 0°, 5°, 10°, 20°$.

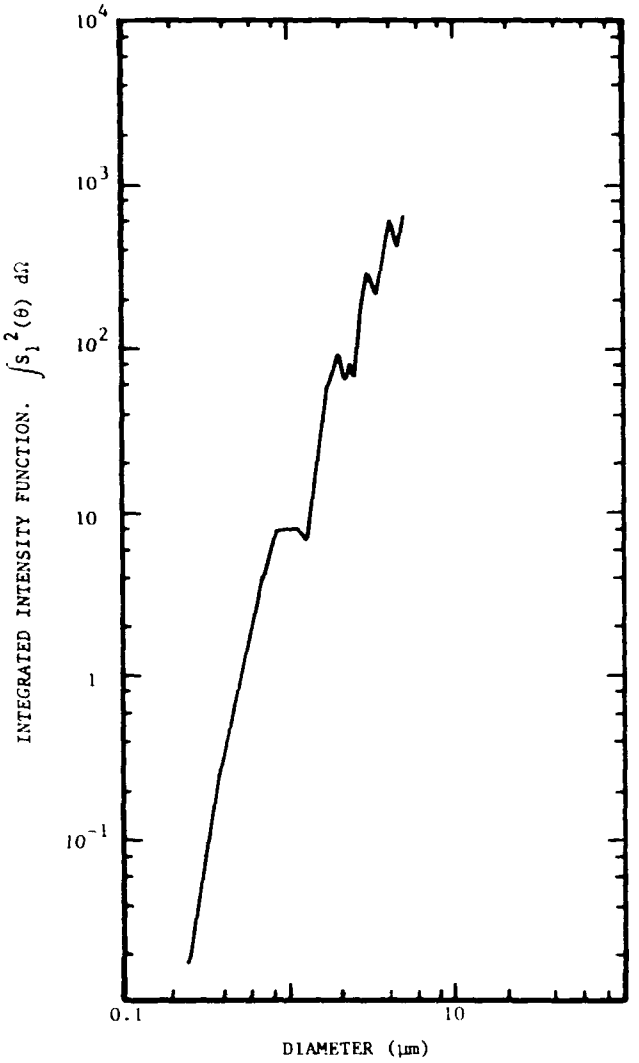

Fig. 5 Integrated intensity function for $\theta = 5°$ and F/5 lens for polystyrene microspheres, ($\tilde{n} = 1.59$) as a function of diameter.

(dn_1/dT) is about 10^{-5} $1/K$[11] and therefore, we should expect small variations of n_1 in the rocket plume.

Since the testing and calibration of the system will be conducted with known size polystyrene particles, the scattering function corresponding to these particles was also evaluated. The results are shown on Figure 5 and, as before, the shallow angles offer the best conditions.

Experimental Setup

Figure 6 shows a schematic diagram of a system using plane laser sheets to measure the size and velocity of particles in a flow. Mirrors M1 and M2 steer a He-Ne laser beam into a beam splitter BS. The separation of the two beams from the beam splitter can be adjusted by changing the position of the input laser beam. By rotating the beam splitter the angle between the two beams can be adjusted. Two cylindrical lenses CL1 and CL2 expanded one dimension of the laser beams into plane sheets. Another cylindrical lens CL3 focused and crossed the two laser sheets at their beam waists. The two laser beams were terminated by beam stoppers. Light scattered from particles crossing the probe volume was collected at 5° by lenses SL1 and SL2 of focal lengths 305 mm and 762 mm, respectively. The collected scattered light was focused on a 400 μm diameter pinhole in front of a photomultiplier tube (EMI 9781R) thus limiting the field of view of the probe volume. This insures a constant laser intensity along the slit width. The PMT was then connected to a VP1001 signal processor which was interfaced to a computer. The velocity of the particles was measured from the frequency of Doppler bursts. The size of the particles was obtained form the peak of the absolute scattered light using a pulse height analyzer interfaced to the frequency counter. A criterion was also set by the signal

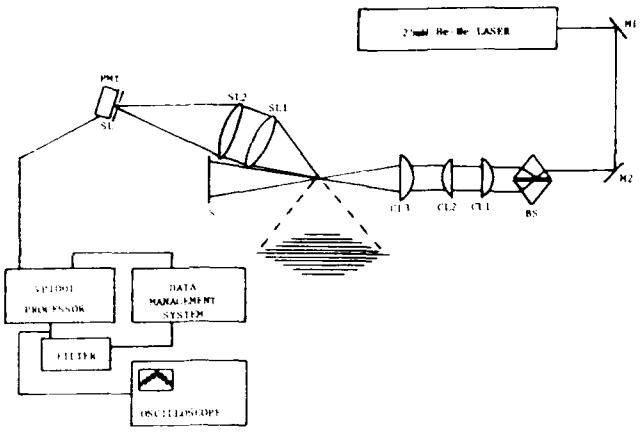

Fig. 6 Schematic Representation of Experiment.

processor to reject optical noise and to limit the detection of the scattered light to particles in the probe volume. A low pass filter eliminated the ac component of the signals measured by the pulse height analyzer.

Results

Two approaches were used to produce known size particles to calibrate the system and estimate the S/N. The first consisted of using a Berglund-Liu monodisperse droplet generator which is capable of producing a string of equal size droplets. Figure 7 shows a typical size/velocity histogram of this monodisperse distribution. The droplet size in this case is 41 μm, which is much larger than the size range of interest for rocket plume diagnostics. Since, these droplets are large (40 to 60 μm), they were only used to align the optics and obtain some simulated conditions by masking the receiver and limiting the collected scattered light. Thus, particles of different sizes could be simulated and the S/N established.

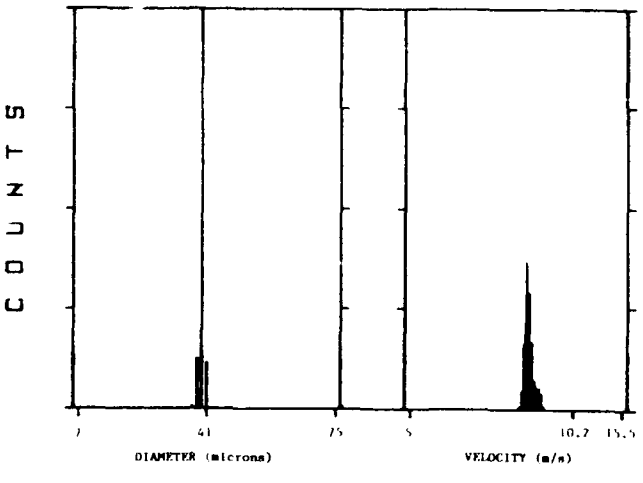

Fig. 7 Monodisperse droplets from Berglund-Liu droplet generator of diameter of 40.8 μm.

The S/N study was conducted at various gain and threshold levels yielding the conditions where satisfactory measurements could be made. Note that the detection criterion is based on the ability of the ac signal to produce N fringes above the threshold with a frequency stable to within an error established by the electronics. Normally, this ac signal results from the fringes which limit the probe volume. It was, however, found that for signals with large optical noise, the light scattered from a single beam could produce sufficient ac content that would fool the electronics and be processed. Figure 8 shows the threshold as a function of diameter for different high voltages to the photomultiplier. The diameter shown is the abscissa normalized to unity and represents the relative position within the size histogram. This result indicates that an intense light source and a low PMT voltage will be required to obtain a large dynamic size range given a specified threshold level.

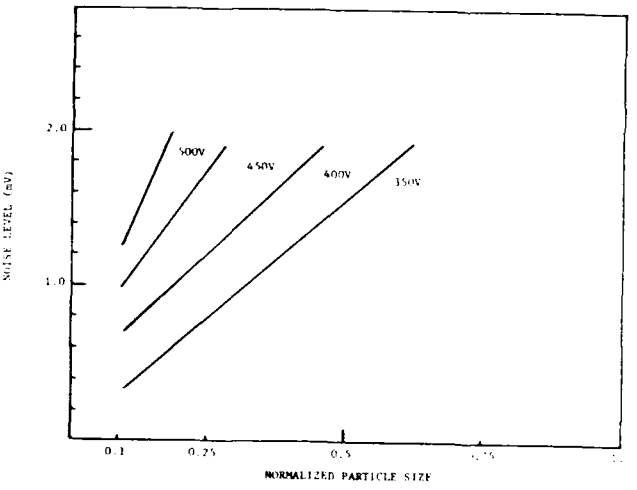

Fig. 8 Noise level as a function of particle size for different PMT voltages.

The second approach consisted of blowing polystyrene particles of 1.1 μm to 3.3 μm in diameter. These particles were first diluted in distilled water. A nebulizer powered by an air compressor was then used to inject the water mist together with the polystyrene particles into a heating chamber. There the water mist was evaporated and the solid polystyrene particles were blown (by the same air compressor) into the probe volume. This allowed the measurement of known size particles in the size range of interest. Different size particles could be diluted in water thus producing more complex distributions such as bimodal and trimodal.

Figure 9 shows typical histograms (size and velocity) of the 1.7 μm particles. Figure 10 shows the results corresponding to a bimodal distribution of 1.1 μm and 1.7 μm, and Figure 11 shows a trimodal distribution of 1.7 μm, 2.7 μm, and 3.3 μm. It should be noted that the high voltages to the PMT in Figures 10 and 11 are different and, therefore, the location of the 1.7 μm is shifted. We had to do this because, in order to measure the 1.1 μm, the high voltage had to be increased. This high voltage was, however, not compatible with the 3.3 μm particles since, for the limited laser power used in these experiments (25 mW of red light), the 3.3 μm signal would have been much broader due to excess noise.

The theoretical relative sizes obtained from the Mie codes are shown on the histograms. For the most part, the peaks are within 10% of the predicted ones which is consistent with some of

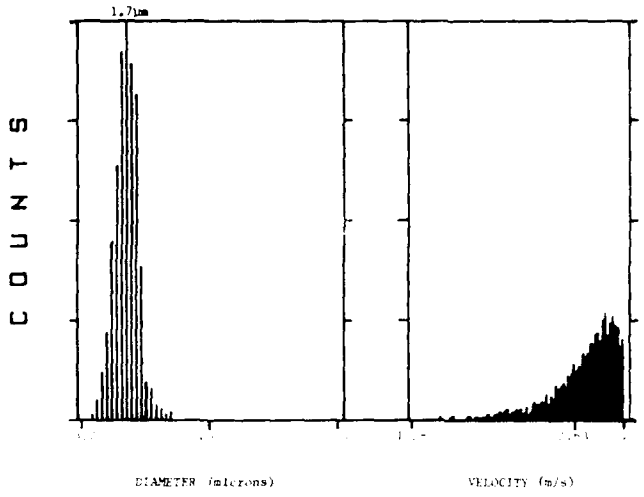

Fig. 9 Histograms of monodisperse polystyrene microspheres of 1.7 μm in diameter.

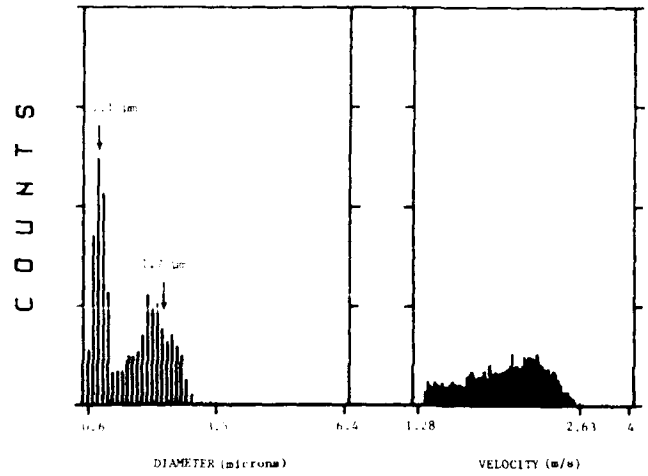

Fig. 10 Histograms of bimodal polystyrene microspheres of 1.1 μm and 1.74 μm in diameter (arrows indicate the relative theoretical diameters).

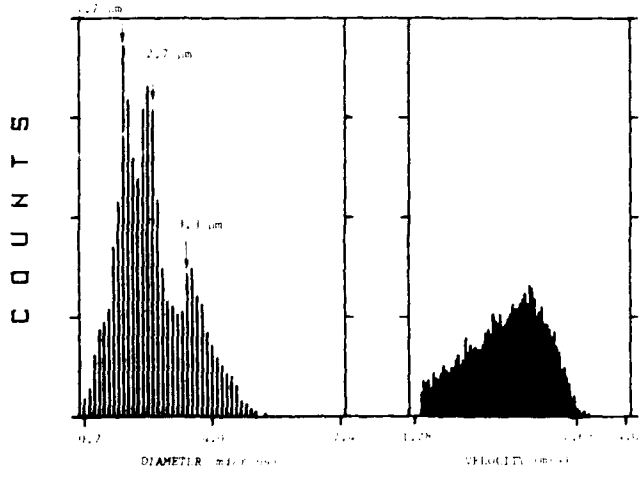

Fig. 11. Histograms of trimodal polystyrene microspheres of 1.7 μm, 2.7 μm and 3.3 μm in diameter (arrows indicate the relative theoretical diameters).

the ambiguities experienced by the scattering function. It can be observed in the histograms that the size distribution of the larger particles is broader. This broadening would be considerably reduced with a more powerful laser or more advanced electronic processing. Nevertheless, the results are quite remarkable for a nonintrusive technique making measurements in such complex size range. These results confirm that the technique is extremely promising to perform measurements in a real rocket plume, given the availability of a high power laser and a faster electronic processor.

Acknowledgement

This work was supported by an SBIR Phase I program managed by the Ballistic Missile Office BMO/MYES under Contract Number F04704-84-C-0107.

References

1. P. T. Girata, Jr. and W. K. McGregor, "Particle Sampling of Solid Rocket Motor (SRM) Exhausts in High Altitude Test Cells," AIAA Paper No. 83-0245, January 1983.

2. R. N. Berglund and B. Y. H. Liu, "Generation of Monodisperse Aerosol Standards," Env. Sci. and Tech., 7 147 (1973).

3. H. C. van de Hulst, "Light Scattering by Small Particles," Chapter 8, Dover Publications, Inc., NY 1981.

4. J. Swithenbank, J. Beer, D. S. Taylor, D. Abbot and C. G. McCreath, in Experimental Diagnostics in Gas-Phase Combustion System: AIAA Progress in Astronautics and Aeronautics, B. T. Zinn, ed., AIAA 53-421 (1977).

5. W. M. Farmer, "Measurement of Particle Size, Number Density, and Velocity Using a Laser Interferometer," Applied Optics 11, 2603 (1972).

6. C. F. Hess, "A Technique Combining the Visibility of a Doppler Signal with the Peak Intensity of the Pedestal to Measure the Size and Velocity of Droplets in a Spray," AIAA Paper No. 84-0203 (1984).

7. E. D. Hirleman, "Laser-Based Single Particle Counters for In Situ Particulate Diagnostics," Optical Engineering 19, 854 (1980).

8. C. F. Hess and V. E. Espinosa, "Spray Characterization with a Nonintrusive Technique Using Absolute Scattered Light," Optical Engineering 23, 604 (1984).

9. D. Holve and S. A. Self, "Optical Particle Sizing for in Situ Measurements," Applied Optics 18, 1632-1646 (1979).

10. D. V. Dave, "Subroutines for Computing the Parameters of the Electromagnetic Radiation Scattered by a Sphere," IBM Report No. 320-3237 (1968).

11. D. A. Gryvnak and D. E. Burch, "Optical and Infrared Properties of Al_2O_3 at Elevated Temperatures," J. Opt. Soc. Am. 55, 625 (1965).